SECURITY CLASSIFICATION OF THIS PAGE

REPORT DOCUMENTATION PAGE

Form Approved
OMB No. 0704-0188

1a REPORT SECURITY CLASSIFICATION UNCLASSIFIED	1b RESTRICTIVE MARKINGS NONE
2a SECURITY CLASSIFICATION AUTHORITY 2b 4 **AD-A213 622**	3. DISTRIBUTION/AVAILABILITY OF REPORT APPROVED FOR PUBLIC RELEASE; DISTRIBUTION UNLIMITED.
	5. MONITORING ORGANIZATION REPORT NUMBER(S) AFIT/CI/CIA-88-231
6a. NAME OF PERFORMING ORGANIZATION AFIT STUDENT AT SAN JOSE STATE UNIVERSITY 6b. OFFICE SYMBOL (If applicable)	7a. NAME OF MONITORING ORGANIZATION AFIT/CIA
6c. ADDRESS (City, State, and ZIP Code)	7b. ADDRESS (City, State, and ZIP Code) Wright-Patterson AFB OH 45433-6583
8a. NAME OF FUNDING/SPONSORING ORGANIZATION 8b. OFFICE SYMBOL (If applicable)	9. PROCUREMENT INSTRUMENT IDENTIFICATION NUMBER
8c. ADDRESS (City, State, and ZIP Code)	10. SOURCE OF FUNDING NUMBERS PROGRAM ELEMENT NO. / PROJECT NO. / TASK NO / WORK UNIT ACCESSION NO.

11. TITLE (Include Security Classification) (UNCLASSIFIED)

APPLICATION OF A MASS-CONSISTENT WIND MODEL TO CHINOOK WINDSTORMS

12. PERSONAL AUTHOR(S)
NEIL J. MURANAKA

13a. TYPE OF REPORT THESIS/~~DISSERTATION~~	13b. TIME COVERED FROM _____ TO _____	14. DATE OF REPORT (Year, Month, Day) 1988	15. PAGE COUNT 94

16. SUPPLEMENTARY NOTATION
APPROVED FOR PUBLIC RELEASE IAW AFR 190-1
ERNEST A. HAYGOOD, 1st Lt, USAF
Executive Officer, Civilian Institution Programs

17. COSATI CODES		
FIELD	GROUP	SUB-GROUP

18. SUBJECT TERMS (Continue on reverse if necessary and identify by block number)

19. ABSTRACT (Continue on reverse if necessary and identify by block number)

153

20. DISTRIBUTION/AVAILABILITY OF ABSTRACT ☒ UNCLASSIFIED/UNLIMITED ☐ SAME AS RPT. ☐ DTIC USERS	21. ABSTRACT SECURITY CLASSIFICATION UNCLASSIFIED
22a. NAME OF RESPONSIBLE INDIVIDUAL ERNEST A. HAYGOOD, 1st Lt, USAF	22b. TELEPHONE (Include Area Code) (513) 255-2259 22c. OFFICE SYMBOL AFIT/CI

DD Form 1473, JUN 86 *Previous editions are obsolete* SECURITY CLASSIFICATION OF THIS PAGE

AFIT/CI "OVERPRINT"

APPLICATION OF A MASS-CONSISTENT WIND MODEL TO CHINOOK WINDSTORMS

A Thesis

Presented to

The Faculty of the Department of Meteorology

San Jose State University

In Partial Fulfillment

of the Requirements for the Degree

Master of Science

By

Neil J. Muranaka

June, 1988

APPROVED FOR THE DEPARTMENT OF METEOROLOGY

Peter F. Lester

Francis L. Ludwig

Alison F. C. Bridger

APPROVED FOR THE UNIVERSITY

ABSTRACT

This research examines the applicability of a simple objective analysis technique on a personal computer to determine the detailed distribution of surface winds during strong downslope windstorms. A three-dimensional, mass-consistent, diagnostic wind flow model applicable to complex terrain (COMPLEX) was modified to analyze surface wind fields for two severe chinook windstorms in southern Alberta. The principal modification to the model consisted of specifying the vertical structure of the mesoscale air flow with a quasi-periodic function based on generally known flow characteristics in mountain waves. Specifically, the boundary layer was assumed to be perturbed by a two-dimensional 'hydrostatic wave'. Sensitivity tests were performed to determine the wave length and boundary layer depth which would provide the best estimates of observed surface wind speeds at selected locations. Results of the most successful sensitivity test were then applied to a sequence of hourly data sets for each windstorm case. Space-time analyses of observed hourly averaged wind speeds were implemented to approximate the movement of the hydrostatic wave in each case.

Realistic results were produced in the case study analyses where maximum winds followed the position of the 'hydrostatic wave' trough, with the highest model wind speeds produced when the wave trough was closest to the mountains. Problems caused by the assumed two-dimensional wave structure included unrealistic changes in wind direction at some boundary points where the model flow surfaces passed beneath the terrain surface. Similarly, the intersection of flow surfaces with the terrain occasionally caused wind speed maxima to occur between, rather than over, hilltops as normally observed. The most significant error was found at the base of the terrain slope where windspeeds were underestimated as the hydrostatic wave trough was moved away from the mountains. Recommended improvements include the use of a hydraulic jump-like flow field in place of the hydrostatic wave perturbation in the model flow surfaces, and a more realistic treatment of the neutral boundary layer.

ACKNOWLEDGEMENTS

The author wishes to extend sincere thanks and best wishes to Peter Lester for his invaluable insight and dedication in obtaining the necessary data and literature which greatly facilitated this project. Special thanks also to Francis Ludwig and Roy Endlich who made the task of understanding the inner workings of COMPLEX much easier. In addition, the author would like to thank Alison Bridger and Jack Molodanof for lending their superior computer skills and expertise. Development of the computer graphics would have been impossible without their assistance. A very special thanks also to Leslie Phillips who made this research possible by compiling and digitizing all of the surface wind data for the Chinook Project. Sincere thanks and best wishes to Dan Tredo who first adapted COMPLEX to the IBM PC-AT and provided the author with invaluable assistance. Finally, the author wishes to extend a warm thank you to Donna Hurth for lending her resourceful and superior secretarial talents.

The Chinook Mountain Wave Project and this research were partially supported by a grant from the Murdock Charitable Trust of Vancouver, Washington.

TABLE OF CONTENTS

TABLE OF CONTENTS (continued)

LIST OF FIGURES

LIST OF FIGURES (continued)

LIST OF FIGURES (continued)

LIST OF FIGURES (continued)

LIST OF TABLES

Chapter 1

INTRODUCTION

a. Background

It is well known that the flow of stable air over mountain barriers produces significant disturbances through deep layers downwind of the mountains. On the mesoscale, mountain-induced disturbances include lee waves, rotor circulations, and downslope windstorms. Over the past 50 years, many field studies, theoretical investigations, and numerical modeling studies have contributed significantly to the understanding of these phenomena (e.g., Lyra, 1943; Queney, 1948; Scorer, 1949; Long, 1954; Alaka, 1960; Nicholls, 1973; Ruettner and O'Neill, 1981; Lilly et al., 1982; Smith, 1985).

Downslope windstorms, known in many areas of the world by local names, are either warm (e.g., Alpine Foehn, Rocky Mountain Chinook, Argentine Zonda) or cold (e.g., French Mistral, Yugoslavian Bora) dry and gusty winds from the mountains (Huschke, 1959). The importance of downslope windstorms lies in their role in the global angular momentum balance (Bretherton, 1969; Lilly, 1972) and in potentially serious local effects. For example, downslope windstorms occasionally develop to hurricane-strength ($\geq$ 35 m s^{-1}).

These so called strong downslope windstorms (SDW) are capable of producing widespread damage and severe aircraft turbulence (Lilly and Zipser, 1972; Fingerhut and Lester, 1973; Lilly, 1978; Lester, 1978a; Hoinka, 1985; Lester and Bach, 1986).

In southern Alberta, chinooks are a common occurrence along the eastern slopes of the Canadian Rocky Mountains (Longley, 1967; Lester, 1975, 1976a, 1976b; Giusti, 1987). The warm chinook winds act to ameliorate an otherwise severe winter climate. Population and agriculture distributions clearly reflect the presence of the chinook belt and it follows that accurate prediction of chinook characteristics is an important task for forecasters in that area.

The state of the art of chinook forecasting in Alberta is similar to the status of prediction capabilities elsewhere (Scheetz et al., 1976; Sangster, 1977; Brown, 1986). Synoptic scale flow patterns related to chinook occurrence are well documented and can be predicted with a high degree of accuracy (Lester, 1976a; Drews, 1982), but mesoscale problems still exist. For example, the observational network in southern Alberta cannot resolve mesoscale characteristics of chinook airflow (Lester, 1976a). This is a serious problem since the worst chinook windstorms are driven by mesoscale processes (Lilly and Zipser, 1972; Lilly, 1978; Lester, 1978a). Additionally, the theory of downslope windstorms is incomplete (Durran, 1986a) and

current numerical models are either oversimplified or require computer resources which regional forecast offices do not possess (Peltier and Clark, 1979; Durran, 1986a; Lester, 1987). As a result, precise chinook windstorm details, such as the timing of the onset and the location/magnitude of the strongest winds, cannot be accurately predicted. This problem is magnified in the case of SDWs.

A partial solution to the SDW forecast problem has been found in some areas through the use of special 'mesonetworks' of observation stations. Subsequent analyses of data from such networks (e.g., Lilly and Zipser, 1972; Brinkmann, 1974; Lilly, 1978; Lester, 1978a; Bedard et al., 1981; Mathews et al., 1984) have suggested that SDWs often behave coherently on the mesoscale, i.e., onsets and movements of the windstorms may be extrapolated over time and space scales of a few hours and several tens of kilometers. These results indicate that regular mesoscale 'nowcasts' and short range forecasts are possible given detailed observations of mesoscale flow.

One difficulty with this solution in Alberta is that network costs would be prohibitively high because of the large area of the chinook belt and the complexity of the terrain. It is proposed here that this difficulty can be overcome by combining a moderately dense, but affordable station network with an accurate, fast, and economical interpolation scheme which takes into account the complexity

of the terrain. Recent advances in objective wind analysis techniques for complex terrain indicate that this proposal is feasible (e.g., Endlich, 1967; Sherman, 1978; Bhumralkar et al., 1978; Endlich and Lee, 1983; Ludwig et al., 1985; Tredo, 1987). In addition to these developments, the Alberta Chinook Project (Lester, 1985; Lester and Phillips, 1987) has produced a series of windstorm data sets which are suitable for mesoscale analysis. Thus, the objective of this study is to investigate the feasibility of analyzing severe chinook windstorms in Alberta with a diagnostic, boundary layer wind model

The investigation is carried out by (i) modifying a state-of-the-art, diagnostic, mass-consistent wind model (COMPLEX) to take into account the influence of mountain lee waves, (ii) testing the sensitivity of the model to those modifications, and (iii) applying the model to two SDW cases. In Chapter 2, observations and theory of downslope winds and mass consistent wind models for complex terrain are reviewed to provide the background for the modification of COMPLEX for mountain wave effects. A description of the procedures used to modify COMPLEX, the case data, sensitivity tests, and experimental procedures are presented in Chapter 3. Results are discussed in Chapter 4, and a brief summary of results, conclusions, and recommendations for future research are presented in Chapter 5.

Chapter 2

LITERATURE REVIEW

a. Downslope Winds

(1) Climatology and Observed Structure

Strong downslope windstorms (SDW) are a subset of orographic flows in which hurricane force winds are produced along the lee slopes of mountains (Brinkmann, 1974; Smith, 1985). Foehn and Bora represent the two general types of downslope winds, which are traditionally classified according to temperature effects (Atkinson, 1981; Durran, 1986a). While SDW may occur with both Bora and Foehn, the former cause temperatures to decrease while the latter produce temperature increases.

Chinook winds are of Foehn type (Brinkmann, 1973). They occur along the entire length of the Rocky Mountain chain and have been studied in detail in southern Alberta (Longley, 1967; Brinkmann and Ashwell, 1968; Holmes and Hage, 1971; Kellie, 1972; Lester, 1975, 1976a; Giusti, 1987) and in Colorado (Ives, 1950; Julian and Julian, 1969; Miller et al., 1974; Brinkmann, 1974; Scheetz et al., 1976).

The chinook of southern Alberta is well-defined because the Arctic front with its extreme temperature contrasts often lies in that area (Mathews et al., 1986). As storms move across the area, the alternation between cold arctic air and warm chinook conditions is dramatic and frequent.

Lester (1975, 1976b) has quantified the traditional description of the chinook (i.e., a warm, dry, gusty wind from the mountains associated with rapid temperature changes) to derive a chinook climatology for Calgary, located in southwestern Alberta. From five years of data (1971-1976), he found that chinooks occurred on an average of 13.5 days each month during October-March. A 'typical' (median) Alberta chinook had a duration of 8 h, minimum relative humidity near 40%, wind direction WSW-WNW, and hourly averaged wind speed of 8 m s^{-1} with maximum gusts to 17.5 m s^{-1}.

Lester (1976b) showed that, for Calgary, the frequency of 'extreme' chinook windstorms (i.e., those with gusts $\geq$ 25 m s^{-1}) was 8% between October and March. For the same months, but for 1978-1984 at a location in the foothills west of Calgary, Giusti (1987) determined that 13% of chinook windstorms could be classified as 'extreme'. He found that windstorms occurred more frequently during the afternoon, although this tendency was less distinct for the strongest windstorms. Also, windstorm durations were less than four hours for more than half the cases.

Individual chinook windstorms are characterized by their intermittency in space and time, i.e., variations in movement and gradients in intensity. Records of wind speed from severe chinook windstorms (Lilly and Zipser, 1972; Brinkmann, 1974; Lester, 1978a; Mathews et al.,1986) show that space and time scales of the chinook winds, SDW, and

wind gusts span a wide range. On the largest scales are the chinook winds (i.e., warm, dry, winds from the mountains with speeds of several m s^{-1}). The area of influence can extend as far as 350 km away from the Continental Divide (Longley, 1967; Mathews et al., 1984) and over that distance along the divide. These general chinook conditions may last a few days (Lester, 1976b). In contrast, severe chinook windstorms which include SDW have a reduced area of influence and a shorter duration. In southern Alberta, hourly averaged wind speeds exceeding 20 m s^{-1} typically occur in a zone 40-50 km wide near the base of the terrain slope and last 3-4 hours (e.g., Lester, 1978a). On the smallest scales are windy periods of tens of minutes and individual gusts which may last on the order of seconds.

The observed movements of SDWs are quite variable (Lester and Phillips, 1987). In southern Alberta and in Boulder, windstorm locations have been observed to fluctuate up and down the slopes and to move steadily out into the plains toward the east (Brinkmann, 1974; Lester 1978a). In both regions, gradients in windstorm intensity are highest at the base of the terrain slope. Lester (1976a) reported that the onset of the chinook in southern Alberta is often marked by wind speed maxima immediately to the lee of the mountains. A similar observation was reported for Boulder by Brinkmann (1974) from her analysis of twenty cases in which gusts exceeded 33 m s^{-1}. A dominant feature of the

Boulder surface winds was a large peak in wind speed at the foot of the mountains with rapid decreases (50% over a distance of 10 km) to the east and west.

(2) Causes of Strong Downslope Windstorms

Severe chinook windstorms are the result of the interaction of circulations with a wide range of horizontal scales (Lester, 1975, 1978a; Lilly, 1978). For example, in Alberta, chinook windstorms occur when the planetary wave pattern produces strong, nearly zonal tropospheric flow of anomalously warm air across the Canadian Rocky Mountains. This cross-mountain flow is intensified by embedded, rapidly moving, baroclinic wave disturbances. These conditions are manifested by an intense surface cyclone in the Gulf of Alaska and a ridge of high pressure building in the state of Washington. Low pressures dominate in northern British Columbia (B.C.) and along the lee of the Rockies in Alberta (Lester, 1976b). As a frontal system crosses B.C. and approaches the Continental Divide, pressure falls along the lee slopes and rises in southeastern B.C. These events lead to the formation of a ridge of sea level pressure over southern B.C. (Brinkmann, 1969), a common synoptic feature of the chinook known locally as the "Foehn nose".

On the mesoscale, the causes of downslope windstorms are tightly linked to large-amplitude mountain lee waves forced by the previously discussed synoptic flow conditions (e.g., Long, 1954; Houghton and Kasahara, 1968; Klemp and

Lilly, 1975, 1978; Clark and Peltier, 1977; Peltier and Clark, 1979; Blumen and Hartsough, 1985; Durran, 1986a, 1986b). Mountain lee waves are stationary gravity waves which form downwind when the stable airflow is displaced vertically by an orographic barrier (Durran, 1986a).

Over the past 30 years, three theories have been advanced to explain the role of lee wave phenomena in SDW development. These are (i) hydraulic jumps, (ii) partial reflection of upward propagating waves, and (iii) trapping of energy by self-induced critical layers.

According to the hydraulic jump theory (Long, 1954; Houghton and Kasahara, 1968), strong winds develop along the lee slope as the fluid undergoes a transition from upstream subcritical flow to supercritical flow over the mountain (Durran, 1986a). The strength of this theory is that the nonlinearity introduced by finite terrain barriers is explicitly accounted for. However, hydraulic jump theory suffers from the unrealistic requirement that the fluid top must be bounded by a rigid lid or free surface. As a result, the vertical propagation of energy which is observed to occur in large amplitude mountain waves cannot be included in this theory.

The partial reflection of vertically propagating waves as a factor in SDW development was investigated by Klemp and Lilly (1975, 1978) using a three-layer, linear, two-dimensional, hydrostatic model with bell-shaped terrain (Durran,

1986b). Upward propagating waves are influenced by the wind and stability profiles as defined by the Scorer parameter (ℓ^2), where

$$\ell^2 = (N/U)^2 - 1/U(d^2U/dz^2) \quad , \quad (1)$$

$$N^2 = (g/\theta_o)(d\theta/dz) \quad , \quad (2)$$

N is Brunt-Vaisala frequency, U is mean horizontal wind speed, g is the gravitational constant, θ_o is a reference potential temperature, and $(d\theta/dz)$ is the mean vertical potential temperature gradient. If the wave encounters a region in which ℓ^2 changes rapidly with height, part of the wave energy may be reflected downward. As a result, the wave amplitude below the reflecting layer is determined by the superposition of the upward and downward propagating waves. For the special case of a three-layer atmosphere flowing over sinusoidal topography, Klemp and Lilly found that the optimal superposition occurs when the vertical dimension of each lower layer is one-fourth of the vertical wavelength. Applying a multi-layered numerical model to the Boulder region, they achieved reasonable success in predicting downslope winds from upstream soundings. Their multiple layer approach has the advantage that with a sufficient number of layers, the mean state can be configured for a close match with an actual sounding. Blumen and Hartsough (1985) improved the Klemp and Lilly approach with a continuous model for partial reflection. However, it must be kept

in mind that because the basic Klemp-Lilly model is linear, caution must be exercised in its application to large amplitude waves where the perturbation fields are comparable in magnitude to the mean flow.

Nonlinear and non-hydrostatic effects from large-amplitude mountain waves on SDW development were investigated by Clark and Peltier (1977) and Peltier and Clark (1979) using a two-dimensional model with bell-shaped terrain (Durran, 1986b). They concluded that if the mountain wave amplifies and overturns (breaks) just above the tropopause, the wave energy becomes trapped between the ground and the level of breaking. The overturning region is interpreted as a self-induced critical layer, and is characterized by the production of locally superadiabatic regions, strong mixing, and a local wind reversal. The trapping of the wave energy produces a large amplitude wave which efficiently transfers large amounts of momentum to the surface, producing a SDW. Their approach explicitly accounts for nonlinear and non-hydrostatic effects, but it has the disadvantage that the interpretation of the complex interaction of several processes is sometimes difficult. Although controversy still exists about the role of self-induced critical layers on wave amplification (Lilly and Klemp, 1980; Peltier and Clark, 1980), it is generally accepted that non-linear effects are important (Durran, 1986a).

(3) Role of Mesoscale Waves in Alberta Strong Downslope Windstorms

Although no comprehensive measurements have been made of the three-dimensional mesoscale structure of SDWs in Alberta, much indirect evidence has been gathered in support of a significant role for mountain lee waves in SDW production in that area. From a 12 year record of lenticular and rotor cloud observations at Pincher Creek in southwestern Alberta, Lester (1978b) deduced a very high frequency of lee waves. He found that lee wave clouds occur on an average of 141 days annually and on 50% or more of the days during the most active months (October and February).

The presence of 50-100 km lee waves (i.e., those which are likely to be hydrostatic) during chinook situations was first documented by Holmes and Hage (1971). Using instrumented aircraft, they found that large snowmelt areas were produced in the troughs of waves that had carried warm air downward, displacing very cold air at the surface. In a particular case (18 January 1968), the wavelengths ranged from 64-67 km and the wave amplitude was estimated at 500-700 m.

Other evidence of long lee waves in the area was given by Kellie (1972) who applied spectrum analysis to data from two instrumented towers in Calgary. He found eastward progressing waves with lengths of 29 to 118 km.

Lester (1975, 1976a, 1976c) and Lester and McPherson (1977) have used aircraft, satellite, and surface observations used to show that the "chinook arch," a distinctive lenticular cloud that often extends hundreds of kilometers along the lee of the mountains, lies in the crest of a gravity wave with a length of 50-100 km. Furthermore, they found that the waves often propogated eastward from the mountains with a phase speed less than the windspeed. Occasionally, observations of multiple chinook arches suggested the presence of at least two long waves downwind of the mountains.

Lester (1976d) documented the high frequency of occurrence of chinook arches (and, therefore, very long lee waves) observed from Calgary during 16 months in 1974-1976. Arches were observed on 132 days with frequencies as high as 15 days per month in December and January. He also found that the relationship between arch occurrence and gusty chinook winds was very strong in the mountains, but decreased significantly to the east. For example, at Kananaskis Forestry Experiment Station, about 10 km east of the Continental Divide, 92% of the arch clouds (25 cases) occurred with gusty chinook winds, while at Calgary, the percentage decreased to 48%. At this time, no clear relationship has been established between the appearance of the chinook arch and the occurrence of SDW.

In a recent climatological study, Giusti (1987) examined soundings taken immediately upstream of the Continental Divide just prior to chinook windstorms. He stratified static stability profiles by observed chinook wind speed categories for several years of data and found that the strength of the wind storm increased with an increase of static stability at mountain top. A similar structure has been associated with Colorado windstorms (Brinkmann, 1973) and agrees with theoretical stability structures that Klemp and Lilly (1975) have found to be conducive to SDW.

The evidence for the importance of non-hydrostatic waves and non-linear effects in the production of chinook windstorms in Alberta is not as extensive as that for the hydrostatic lee wave. A recent paper by Lester and Bach (1986) examined an extreme clear air turbulence incident which occurred near the tropopause during an SDW event approximately 50 km west of Calgary. Satellite data and derived aircraft records of vertical velocity and potential temperature showed that both long (50-100 km) hydrostatic lee wave, and shorter (10-20 km) non-hydrostatic mountain lee waves were present. Furthermore, an extensive turbulent layer which existed near the tropopause was suggestive of the critical layer necessary for wave energy trapping, as hypothesized by Peltier and Clark (1979).

b. Mass-Consistent Wind Models

Even with recent advances in downslope wind theory, analysis of surface wind fields associated with SDWs remains a difficult problem (e.g., Blumen and Hartsough, 1985; Smith, 1985; Durran, 1986a). The numerical models developed by Klemp and Lilly (1975), Peltier and Clark (1979), and Durran (1986a) simulate the dynamics of mountain airflow, and can produce mountain wave patterns consistent with observations. However, their use of smoothed topography limits direct application of those models to boundary layer wind flow because smaller scale flow perturbations due to complex terrain are not included. As noted in Chapter 1, the current investigation will attempt to overcome the latter problem by the adaptation of a diagnostic wind model to yield physically reasonable hourly objective surface wind analyses during SDW events.

Mass-consistent wind models (e.g., Sherman, 1978; Bhumralkar et al., 1978) are objective boundary layer wind analysis schemes which are applicable to regions of complex terrain and require only modest, readily available computer resources (Tredo, 1987). In the most sophisticated of these models, wind observations are interpolated to a three-dimensional grid and then adjusted so that conservation of mass is satisfied. The accuracy of the final wind field is dependent upon the number and quality of wind observations, and on the representation of physical processes by the model

inputs (Mass and Dempsey, 1985; Tredo, 1987).

One of the earliest diagnostic wind models was the mass-adjusted, three-dimensional wind flow model for complex terrain (MATHEW) developed by Sherman (1978) from the continuity equation in rectangular coordinates (Ludwig, 1987). In MATHEW, a variational method by Sasaki (1958, 1970) was used to minimize differences between the initial wind analysis derived from observed values and the final mass-consistent flow. A power law was used for vertical profile estimates. Practical use of MATHEW is difficult because the rectangular coordinates complicate the problem of specifying meteorologically satisfactory boundary conditions, especially at the lower boundary (Endlich, 1967; Ludwig, 1987).

In the COMPLEX mass-consistent wind model developed by Bhumralkar et al. (1978), the sigma (σ) system is incorporated to produce an initially terrain-following coordinate system.

$$\sigma = [z - h(x,y)]/[H(x,y) - h(x,y)] \quad , \qquad (3)$$

where z is height above sea level, h is height of terrain above sea level, and H is the height of the boundary layer top. The lower boundary condition is specified by the terrain height while the upper boundary (boundary layer top) is given by the equation:

$$H(x,y) = Z + sh(x,y) + (1 - s)h_o \quad , \qquad (4)$$

where Z is the average boundary layer thickness, s is a "slope" factor, which defines the degree to which the boundary parallels the underlying terrain, and h_o is the terrain height at a specified reference point. The use of sigma coordinates allows for simple formulation of the upper and lower boundary conditions as the terrain and boundary layer top are assumed to be impermeable boundaries. Observations of horizontal wind from scattered stations are interpolated to a horizontal grid and extrapolated vertically to each sigma level.

More recently, COMPLEX has been modified to include (i) the use of the geostrophic wind to represent upper boundary flow (Endlich et al., 1980, 1982), (ii) the incorporation of critical streamline concepts to convert from a terrain-following to a flow-following coordinate system (Endlich and Lee, 1983; Ludwig et al., 1985), and (iii) the inclusion of an iterative (rather than variational calculus) procedure to eliminate divergence in the wind field (Endlich, 1967; Endlich et al., 1980). These changes are described below.

The geostrophic wind is applied at a specified maximum height above the terrain unless the boundary layer top is below the mountain tops, so that the influence of the underlying terrain is limited to a shallower layer. The critical streamline concept (Hunt and Snyder, 1980) involves the balance between the potential energy gained from vertical motions in a stably stratified atmosphere and the kinetic

energy of the horizontal motion (Ludwig et al., 1985; Ludwig, 1987; Tredo, 1987). At the critical streamline height, kinetic energy of the flow equals the potential energy gained by raising air parcels to the top of a terrain obstacle. The governing relationship for a stable, adiabatic atmosphere in which vertical displacements are small can be written as

$$\frac{V_o^2}{2} = \frac{g}{T_m} \int_{z_o}^{z_{MAX}} (z - z_o) \frac{\delta\theta}{\delta z} dz \quad . \quad (5)$$

The left side is the kinetic energy (per unit mass) of the flow while the right side is the potential energy (per unit mass) gained by lifting the air from Z_o to the height, Z_{MAX}. $\delta\theta/\delta z$ is the vertical gradient of potential temperature, and T_m is the average temperature through the layer. Integrating the right side of Eqn. (5) gives the highest rise for the flow against the existing lapse rate,

$$Z_{MAX} - z_o = V_o \left[(g/T_m)(\delta\theta/\delta z)_o\right]^{-\frac{1}{2}} \quad , \quad (6)$$

where $(\ )_o$ refers to conditions at the lowest geometric level. Air above/below the critical streamline height proceeds over/around the obstacle, provided that wind increases with height. In the model, the highest obstacles over which the air can flow are defined. Then sigma levels are reassigned from terrain-following to flow-following based on

this critical streamline concept. Wind speed over the lower terrain elevations and lapse rates at the various sigma levels form the basis for this definition of flow surface shape.

Once the flow-following surfaces are determined, divergence is eliminated using an iterative procedure (Endlich, 1967; Endlich et al., 1980) in which horizontal wind components on volume elements (Fig. 1) are sequentially adjusted to balance mass inflow with outflow (Tredo, 1987). Each volume element is bounded at the top and bottom by flow surfaces so that inflow or outflow from each element can occur only through the vertical faces. The divergence (D) for a volume element is given by

$$D = (\delta u^*/\delta x) + (\delta v^*/\delta y) \quad , \quad (7)$$

$$u^* = u \times \delta z \quad , \quad (8)$$

$$v^* = v \times \delta z \quad , \quad (9)$$

where u and v are the horizontal velocity components on the volume element; δz is the vertical separation between two flow surfaces, and u^* and v^* are the respective fluxes for each horizontal velocity component. For example, if convergence is occurring in a volume element due to greater inflow, wind components are adjusted to decrease/increase wind component values on inflow/outflow faces of the volume element until the value of D is zero. However, this adjustment changes the divergence value for adjacent volume

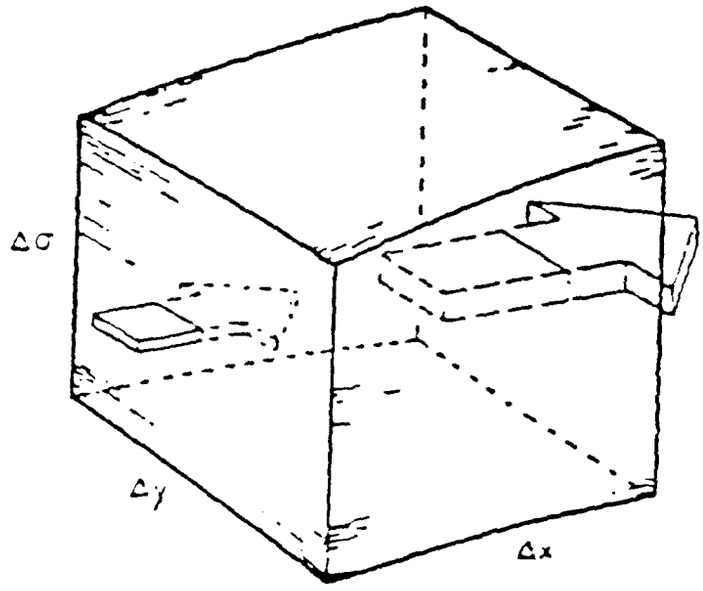

Figure 1. A 'volume element' in the grid mesh (after Endlich et al., 1982).

elements, therefore the procedure is repeated until the divergence in all volume elements is removed. In practice, the iterations are stopped after a specified number have been completed, resulting in small divergence. By making the wind field non-divergent, those boundary conditions that are usually required to solve Poisson equations for stream function and vorticity are not needed.

The final step is to interpolate the mass-adjusted wind components on flow-following surfaces to anemometer height (10 m) above the terrain. A detailed discussion of the coordinate system, initial wind analysis, mass-conservation adjustment, and surface-wind interpolation procedure is presented by Tredo (1987). Steps in the computational procedure (Nitz et al., 1985) are as follows:

1) Specify boundary layer top and terrain-following (sigma) surfaces.
2) Interpolate wind profile and surface winds to sigma surfaces.
3) Make initial (first guess) objective wind analysis.
4) Adjust sigma surfaces to become flow-following surfaces using the critical streamline concept.
5) Remove divergence from wind field.
6) Interpolate mass-adjusted wind field to anemometer height (10 m) above the terrain surface.

Results from investigations of chinook boundary layer structure using acoustic remote sensors (SODARS) near Calgary (Mathews and Hicks, 1979; Mathews et al., 1984) indicate that the onset and cessation of the chinook windstorms is often strongly influenced by the interaction of mountain waves with the surface boundary layer (Lester,

1985). Since COMPLEX has evolved to a point where it can produce mass-consistent wind fields for varied airflow structures (e.g., mountain waves), its application to Alberta chinook SDWs is an appropriate experiment which has not been previously attempted.

Chapter 3

PROCEDURES

a. Modification of COMPLEX for Strong Downslope Windstorms

Despite the past successes of COMPLEX in the analysis of winds in mountainous terrain, the initial application of that model to a chinook windstorm produced unrealistic surface wind patterns. For example, the strongest winds occurred only over the mountain peaks with little enhancement of the winds at the foot of the mountains as is usually observed. This result was due to the fact that COMPLEX (as described in Chapter 2) does not take into account the important influence of mountain lee waves on the boundary layer. In this section, the modification of COMPLEX to reflect the influence of lee waves is described.

As noted in Chapter 2, the critical streamline concept (Hunt and Snyder, 1980) has been used in recent versions of COMPLEX to make the transition from a terrain-following to a flow-following coordinate system (e.g., Tredo, 1987). While this modification introduces more reasonable physics into COMPLEX, it does not incorporate mesoscale forcing of surface winds by mountain waves. In addition, if the assumptions underlying the critical streamline concept do not hold, then the use of flow-following coordinates by COMPLEX requires knowledge of the three-dimensional structure of the flow, including the height of the boundary layer top.

Unfortunately, such observations are not available for chinook SDW cases considered here. Although the Chinook Project has generated several windstorm data sets over the last few years, these sets are mainly composed of hourly surface wind observations (Lester and Phillips, 1987). It follows that some assumptions must be made about the nature of the structure of the flow aloft in order to carry out the proposed experiment for the Alberta SDWs.

Wind profiles have been specified by measuring a 'regionally' representative geostrophic wind at 700 mb (near mountain top level) and then linearly interpolating between that wind and the surface wind. The requirements for the stability profile were simplified by suppressing the critical streamline feature of COMPLEX and ensuring that the flow follows the shape of the upper boundary which was predetermined on the basis of mesoscale flow patterns observed elsewhere during SDW conditions.

The slope of the boundary layer top for COMPLEX and the final flow-following coordinate system was specified with a simple diagnostic model of the mountain lee wave influence. Because of the high frequency of the chinook arch cloud in southern Alberta (Chapter 2), the model is based on the assumption that the SDW cases are driven by a hydrostatic lee wave, i.e., the windstorms are primarily the result of processes described by Klemp and Lilly (1975, 1978).

The basic characteristics of the hydrostatic wave (i.e., wavelength, amplitude) were determined from past simulations and analyses of lee wave systems associated with downslope windstorms (e.g., Lilly and Zipser, 1972; Fingerhut and Lester, 1973; Klemp and Lilly, 1975, 1978; Lester and MacPherson, 1977). Because of the detailed documentation and analysis of the 11 January 1972 SDW in Boulder, Colorado, and because that case apparently captures the major mesoscale wave features of the SDW, it was subsequently chosen as the primary guide for configuring the boundary layer top of COMPLEX. The lower portion of the potential temperature field for the 11 January 1972 case, redrawn from Lilly and Zipser (1972) is presented in Fig. 2a. On the basis of the spatial variation of the lowest stable layer in that analysis, the functions illustrated in Figure 2b and discussed below were used to approximate a two-dimensional, 'hydrostatic wave' disturbance of the boundary layer top. This may be interpreted as a condition in which the model flow surfaces correspond to isentropic surfaces, and where small scale turbulent mixing plays a negligible role. The condition is introduced via:

$$T_{top}(r) = h_{top} + Z_{top} - A \exp(-b[r - \phi_{top}]^2) \quad , \quad (10)$$

$$A = h_{top} + Z_{top} - Z_{base} - h_{base} \quad , \quad (11)$$

where $T_{top}(r)$ is the height (ASL) of the boundary layer top

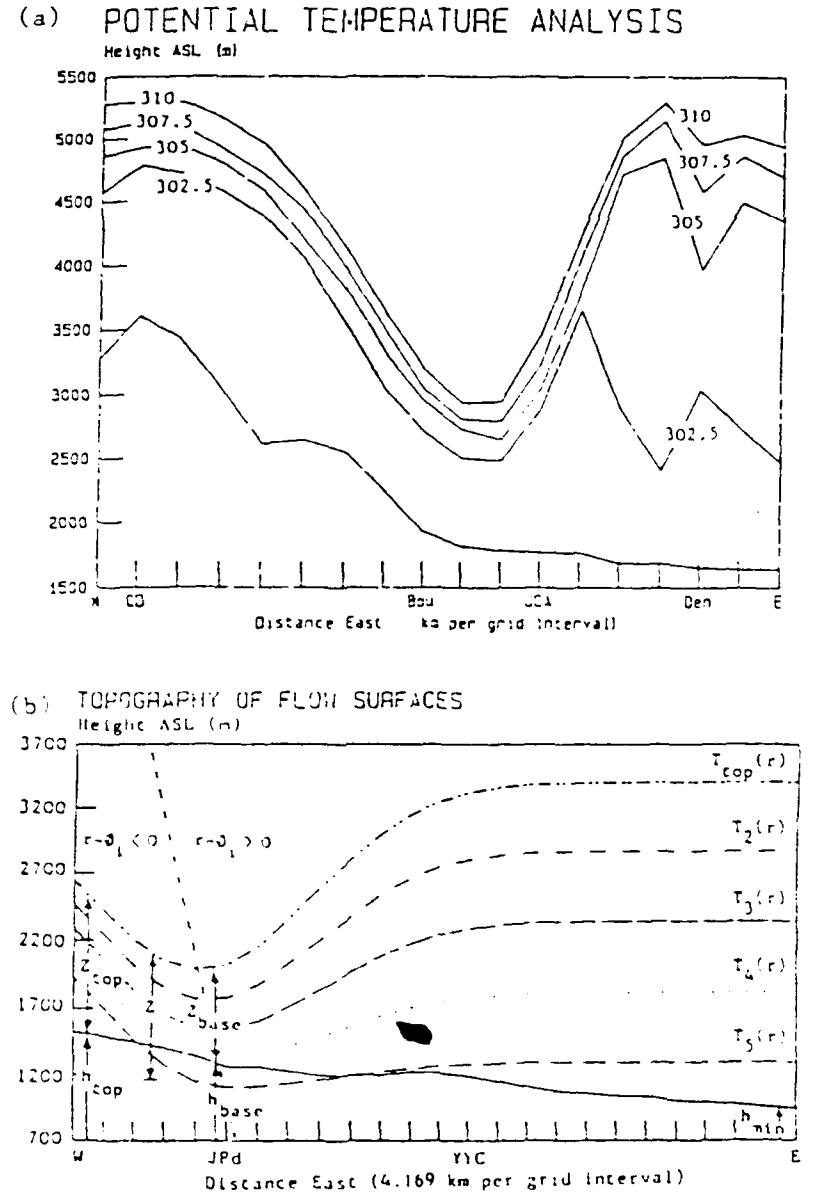

Figure 2. (a) Potential temperature analysis from Boulder windstorm of 11 January 1972 (after Lilly and Zipser, 1972). Potential temperature isopleths are drawn at 2.5 K intervals. The analysis extends from the Continental Divide (CD) through Boulder (Bou), Jefferson County Airport (JCA), and Denver (Den). (b) Schematic cross section of model flow surfaces illustrating terrain height and layer thickness parameters. The upstream tilt of the hydrostatic wave trough axis is represented by a thin dashed line.

at r; r is the normal distance from the wave trough axis (positive east of the trough axis); h_{top}, h_{base} are the terrain heights ASL at the top and base of the slope; Z_{top}, Z_{base} are the boundary layer thicknesses at the top and base of the slope; b is a constant determining the half-width (wavelength) of the wave trough; A is the wave amplitude; and ϕ_{top} is a phase distance constant included so that an upstream tilt in the flow surfaces can be specified. The Gaussian exponential function is chosen because of its symmetry. Furthermore, the symmetry point can be used to represent the mountain wave trough, and the half-width parameter (b) can be easily adjusted to produce disturbances of different wavelengths. Finally, wave phase can be varied as a function of height by adjusting the position of the symmetry point for each flow surface.

The lowest flow surface was set at the lowest terrain elevation within the model domain. Flow surfaces between the boundary layer top and the lowest terrain elevation were specified using:

$$T_i(r) = E_i - A_i \exp(-b[r - \phi_i]^2) \quad , \tag{12}$$

$$E_i = \begin{cases} h_{top} + Z_{top} - [Z(i-1)/(N-1)] & r < 0 \\ [h_{top} + Z_{top} - h_{min}][i-1]/[N-1] & r > 0 \end{cases} , \tag{13}$$

$$A_i = \begin{cases} A & r < 0 \\ A - [E_i(r < 0) - E_i(r > 0)] & r > 0 \end{cases} , \tag{14}$$

where $(\ )_\perp$ specifies the flow surface level; $T_i(r)$ is the height of the ith flow surface ASL; E_i is the equilibrium height of the ith flow surface; A_i is the amplitude of the ith flow surface; h_{min} is the elevation of the lowest terrain point in the model domain; ϕ_i is the phase distance constant for the ith flow surface; N is the number of flow surface levels used in the model (Fig. 2).

Values of boundary layer thickness at the top and base of the terrain slope Z_{top}, Z_{base} (Eqns. (10), (11), (13)), were also derived from the 11 January 1972 Boulder potential temperature analysis (Fig. 2) as a first approximation of the chinook mountain wave flow. Terrain heights at the top and bottom of the slope, (h_{top}, h_{base}) were derived from the terrain data set for southern Alberta in order to scale the wave amplitude to the model terrain. An 18-20° per km upstream tilt (phase change with height) was specified in the model flow surfaces based on a simulation of the 11 January 1972 Boulder windstorm by the Klemp and Lilly (1978). In order to position the mountain wave disturbance, the horizontal axis of the hydrostatic wave trough was aligned parallel to the Continental Divide (337° to 157° true), coincident with the strongest hourly averaged surface winds (this is in agreement with observation and theory). Wave propagation was assumed to occur away from the mountains at an angle normal to the Continental Divide with the wave amplitude remaining constant. Space-time analyses of hourly

averaged wind speeds along the Banff-Calgary corridor were then used to approximate the speed of the wave trough.

In summary, the COMPLEX wind analysis code has been modified by using observed and simulated characteristics of hydrostatic mountain waves to specify the combination of mesoscale forcing of the surface flow features and the mass-consistent adjustments intended to account for smaller scale flow features produced by terrain.

b. Case and Data Selection

Two chinook SDW cases, were selected from the Chinook Project data base: 3 November 1975 and 27 March 1986. Selection criteria were (i) the occurrence of record or near record surface winds over southwestern Alberta, and (ii) the availability of a relatively large data set (Lester and Phillips, 1987). The defined study area (Fig. 3) is located in the lee of the Canadian Rocky Mountains near Calgary, 45-120 km east of the Continental Divide. Upper air data included radiosondes from the northwestern U.S. and southwestern Canada, available pilot reports, and conventional GOES satellite imagery. Hourly surface wind reports were gathered from a variety of sources including conventional first-order surface stations operated by the Atmospheric Environment Service (AES), surface weather stations operated by the University of Calgary (UC), automated weather stations constructed as part of the 1988 Calgary Winter Olympics, and air quality/meteorological data monitoring

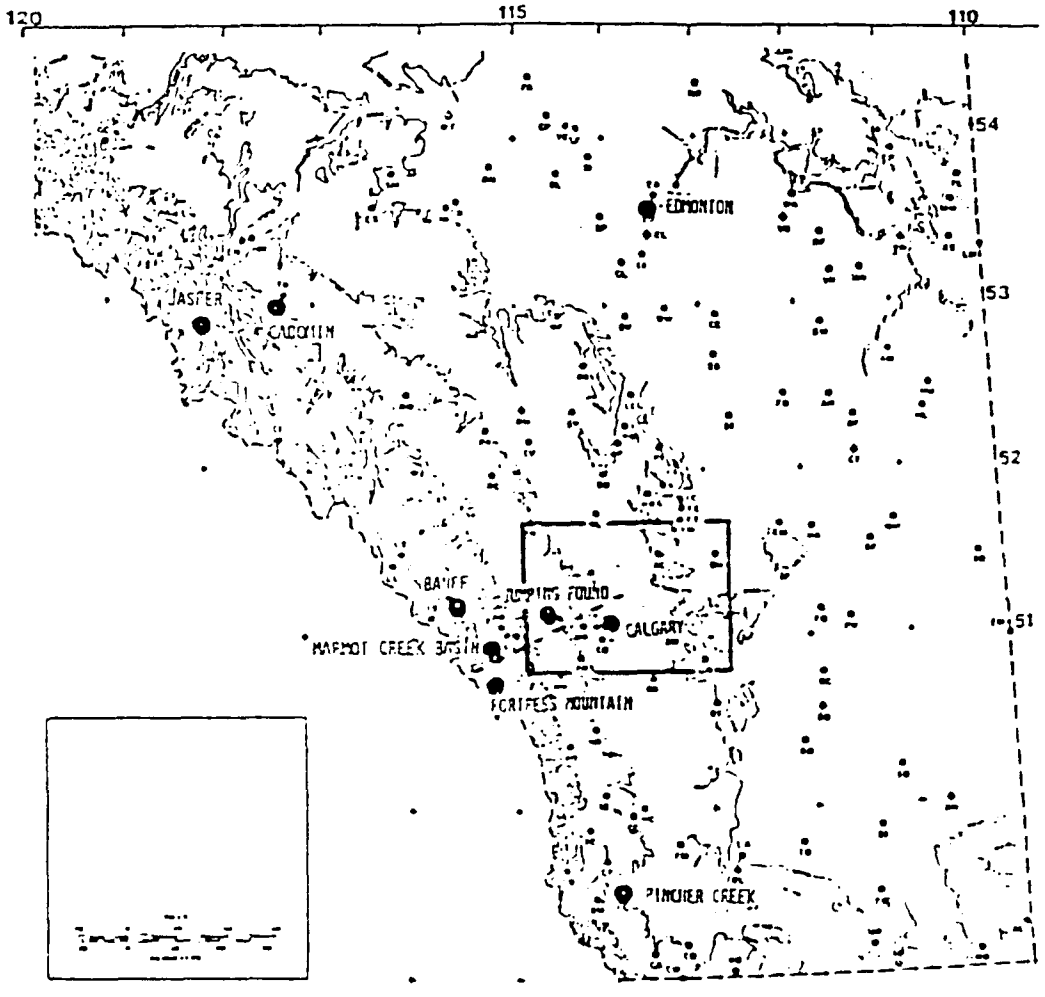

Figure 3. Topographical chart of southwestern Alberta (after Lester, 1978a). The study area is indicated by heavy dark lines while the transect line is indicated by a dashed line.

sites operated by natural gas processing plants. With one exception, data from all of the above sources are subjected to high quality control and considered to be reliable. Site exposures and some quality control procedures for data from gas plants have resulted in less reliable data for some locations. Temporal and spatial consistency were used as the primary tool to accept or reject those data.

Data selected as model inputs from the data base described above are hourly surface wind observations, analyses of upper air flow every 12 hours and terrain elevations. For the majority of the surface wind stations, only eight wind directions (N, NW, W, SW, S, SE, E, NE) were recorded. The average density of surface stations is one per 850 km^2 for the 3 November 1975 case, and one per 600 km^2 for the 27 March 1986 case. These may be compared to the average density of one per 12,600 km^2 for conventional weather stations representing a 15 fold density improvement for the 3 November 1975 case, and a 21 fold density improvement for the 27 March 1986 case. Selected stations for each case are described below.

c. General Meteorological Conditions

(1) 3 November 1975

Synoptic patterns from surface and 700 mb analyses (Fig. 4) for 3 November 1975 at 1400 MST and 1700 MST, respectively, show an intense cross-mountain gradient in mean sea level pressure, relatively warm air aloft (indi-

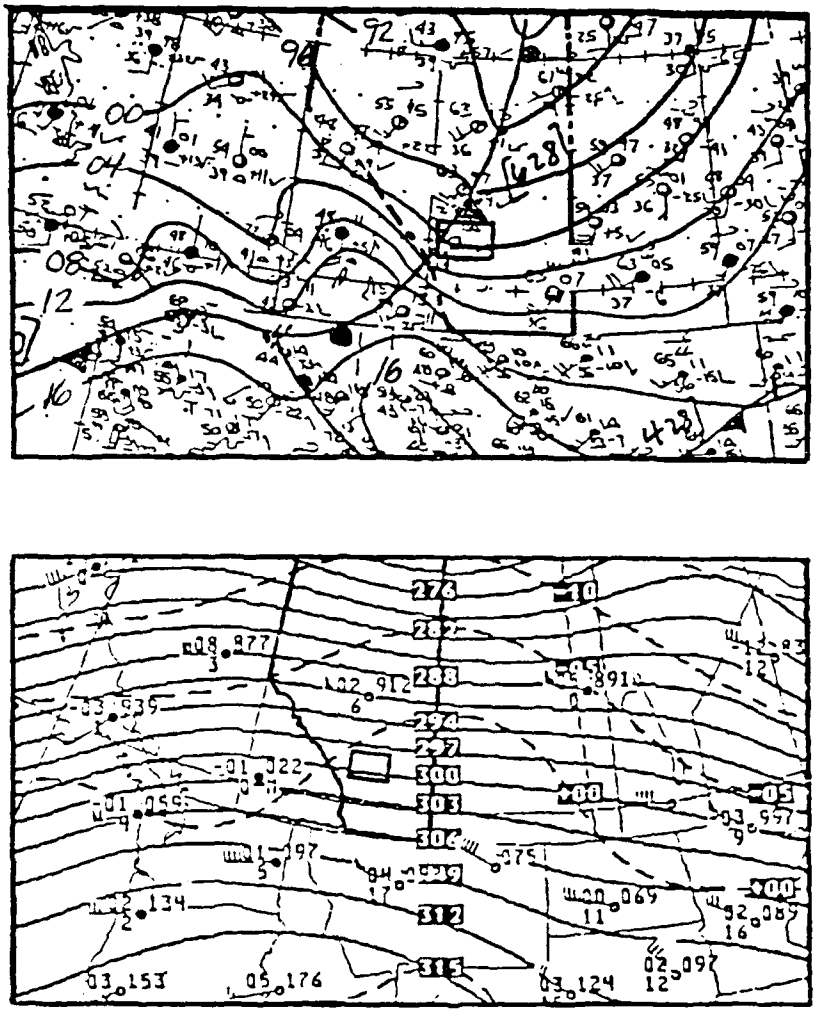

Figure 4. Synoptic analyses (a) surface analysis at 1400 MST and (b) 700 mb analysis at 1700 MST for 3 November 1975. The province of Alberta and the study area are indicated by heavy dark lines. Both (a) and (b) incorporate standard plotting models and conventional labels. In (a), solid lines are isobars at 4 mb intervals. The solid line with triangular pips is a cold front. In (b), solid lines are contours of geopotential height at 30 m intervals while dashed lines are isotherms at 5 C intervals.

cated by ridging of isotherms on 700 mb analysis), and a strong westerly upper air current during the SDW event. Previous analyses by Lester (1978a), Lester and Bach (1986), and Lester and Phillips (1987) reported that the strongest winds occurred with the approach of a rapidly moving baroclinic disturbance from the west. The air mass across southern Alberta was unusually warm for the season, as evidenced by a high tropopause and the location of the major jet stream axis well north of the windstorm area (Lester and Phillips, 1987).

The chinook arch was present on the east side of the Continental Divide over the windstorm area indicating a hydrostatic lee wave of 50-100 km wavelength (Lester and Bach, 1986; Lester and Phillips, 1987). Also present during the windstorm were shorter lee waves (28 km) embedded within the chinook arch. The shorter waves were identified with both aircraft data and satellite observations (Lester and Bach, 1986).

Record surface winds, extensive property damage, and forest blowdown occurred as the windstorm spread eastward from the mountains (Lester, 1978a). Movement of the windstorm at the longitude of Calgary is illustrated in a space-time section of hourly averaged wind speed (Fig. 5) between Marmot Creek Basin (MCB), Kananaskis Research Centre (ESC), Jumping Pound (JPd), and Calgary International Airport (YYC). The space-time sections were produced using spline

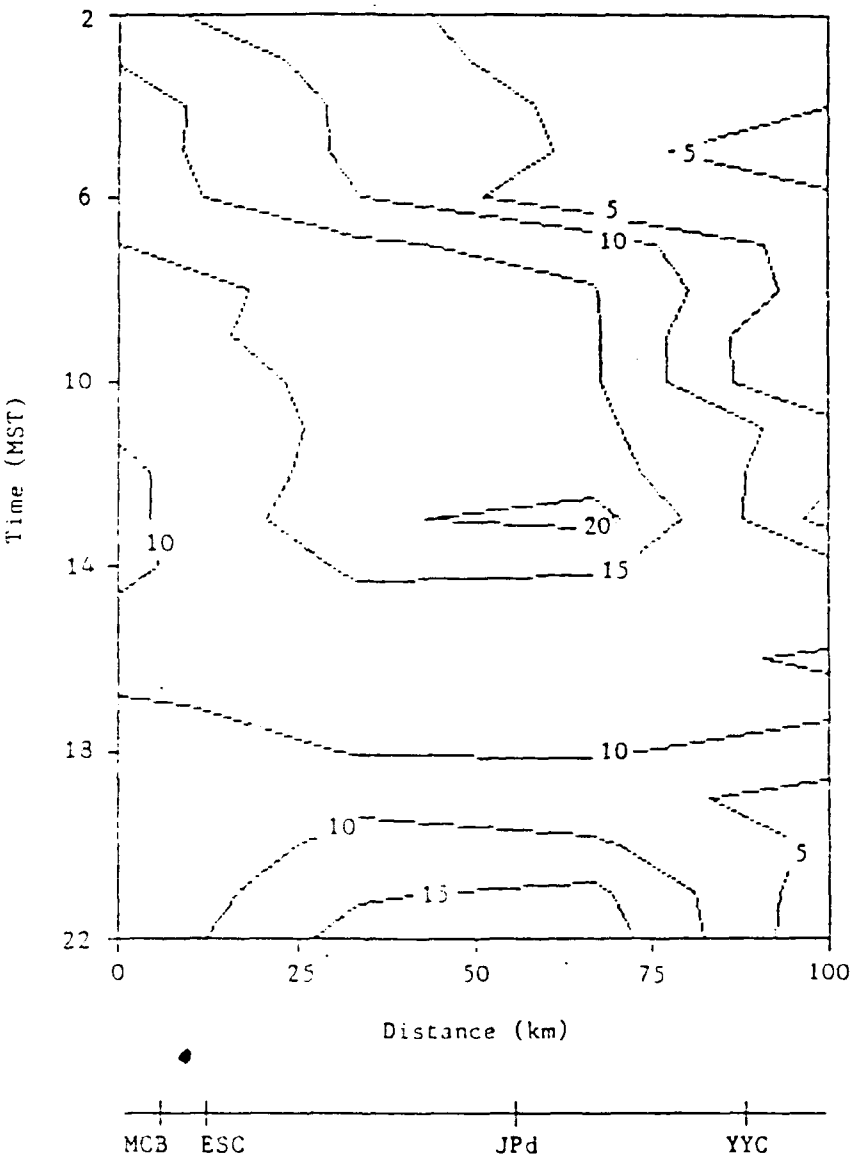

Figure 5. Space-time section of mean hourly wind speed (m/s) for 3 November 1975 along transect line between Marmot Creek basin (MC3), Kananaskis Research Centre (ESC), Jumping Pound (JPd), and Calgary International Airport (YYC). Isotachs are drawn at 5 m s^{-1} intervals, except 25 m s^{-1} is not shown for clarity.

interpolation and applying a single smoothing. The transect line is represented by the dashed line in Fig. 3. Wind speeds exceeding 15 m s^{-1} appeared at MCB at 0600 MST. The windstorm then proceeded eastward reaching its maximum strength with winds exceeding 25 m s^{-1} when it arrived at JPd at 1300 MST (note: for clarity, the 25 ms^{-1} isotach is not shown in Fig. 5). The windstorm reached midway between JPd and YYC at 1400 MST producing winds exceeding 15 m s^{-1}, but by the time it reached YYC at 1500 MST, the windstorm diminished in intensity as wind speed fell below 15 m s^{-1}.

(2) 27 March 1986

Synoptic patterns from surface and 700 mb analyses (Fig. 6) for 27 March 1986 at 1400 MST and 1700 MST respectively are similar to those from 3 November 1975. Again, an intense cross-mountain mean sea level pressure gradient, relatively warm air aloft, and a strong westerly upper air current were present during the SDW event. These conditions were conducive to the production of mountain waves, and, in fact, Lester and Phillips (1987) documented the presence of a chinook arch over the windstorm area.

The space-time section analysis of hourly averaged wind speed between Fortress Mountain (FtM), ESC, JPd, and YYC is shown in Fig. 7. Unlike the 3 November 1975 case, wind speeds at the higher elevations of FtM and ESC were less than 15 m s^{-1}, and stronger winds at lower elevations were observed. The windstorm produced winds exceeding 30 m s^{-1}

(a)

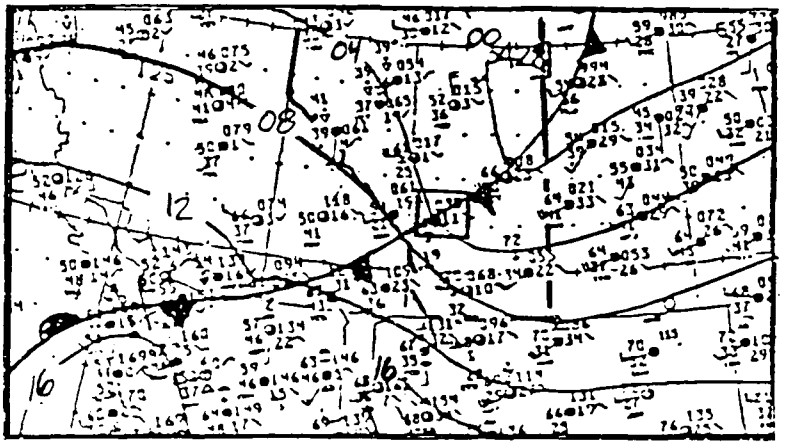

(b)

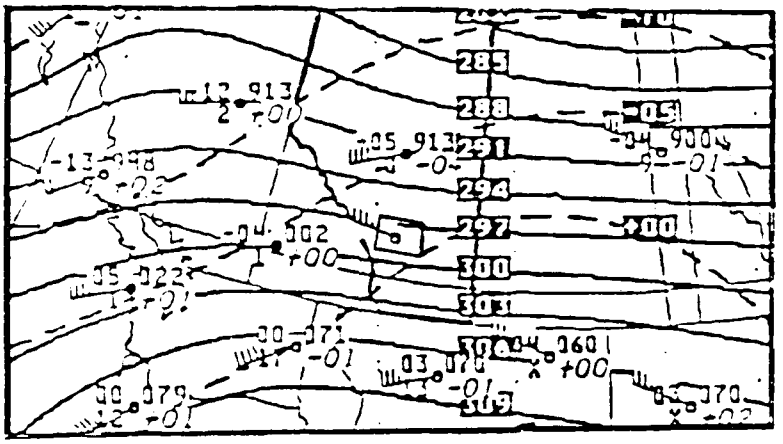

Figure 6. Same as Fig. 4, except for 27 March 1986.

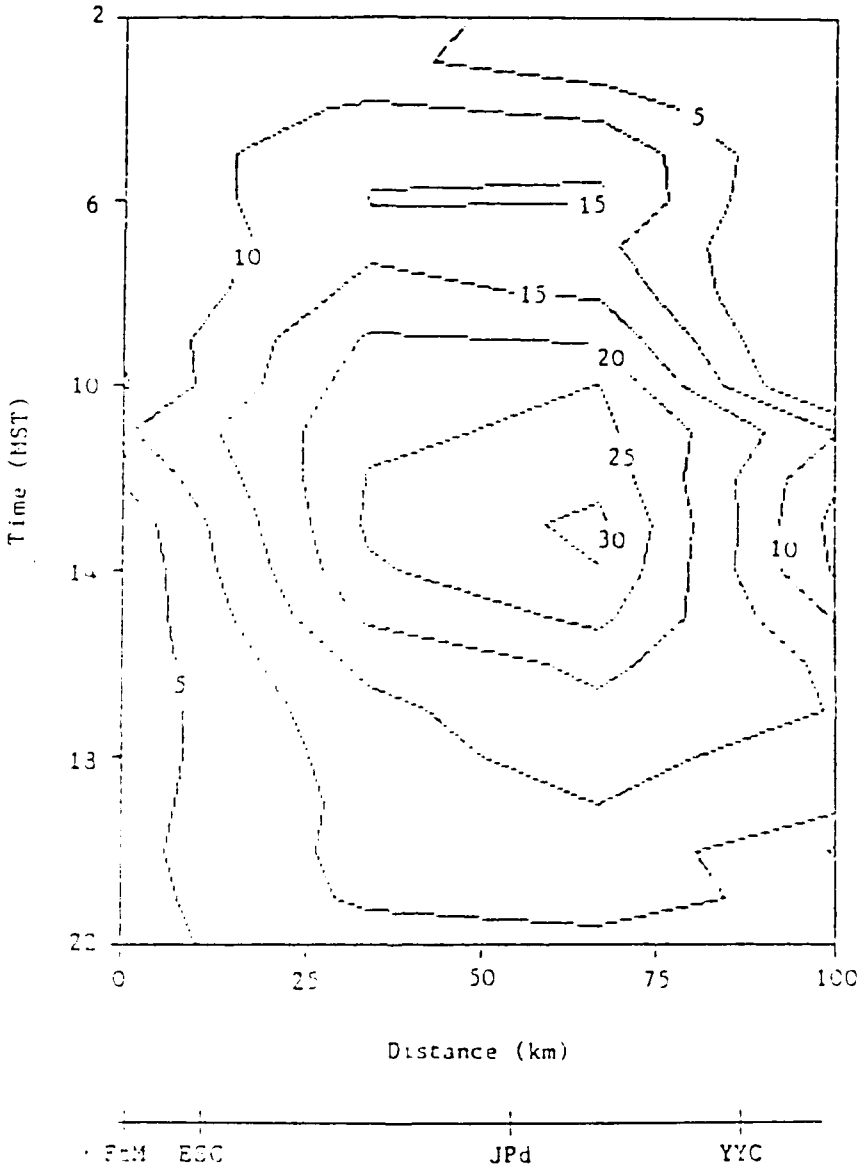

Figure 7. Space-time section of mean hourly wind speed (m/s) for 27 March 1986 along transect line between Fortress Mountain (FtM), Kananaskis Research Centre (ESC), Jumping Pound (JPd), and Calgary International Airport (YYC). Isotachs are drawn at 5 m/s intervals.

when it arrived at JPd at 1300 MST. Winds exceeding 20 m s^{-1} continued as the windstorm reached midway between JPd and YYC at 1400 MST. Winds generally diminished as the windstorm reached YYC at 1600 MST, although wind speed still exceeded 15 m s^{-1}.

d. Application of COMPLEX to SDW Cases

(1) Computational Grid, Terrain, and Station Locations

In the present study, a three-dimensional grid (34x23x6) with a horizontal resolution of 4.169km was specified for the Calgary area for both the 3 November 1975 case and the 27 March 1986 case. The grid interval was selected because the available terrain data were coded in minutes of latitude/longitude and COMPLEX requires that terrain data be arranged in square grid elements.

A three-dimensional perspective of the study area terrain is presented in Fig. 8. The steepest terrain near the Continental Divide was not included in the computational domain to avoid areas with a high probability of non-hydrostatic effects. Important terrain features in Fig. 8 are the Bow River Valley, and the relatively steep secondary slopes lying west of Highway 2 near Crossfield. Maps of the model grid and the surface wind stations for each case are presented in Fig. 9. The eastern portion of the grid is not shown because no surface wind data were available. The names and grid coordinates of each surface wind station are listed in Table 1.

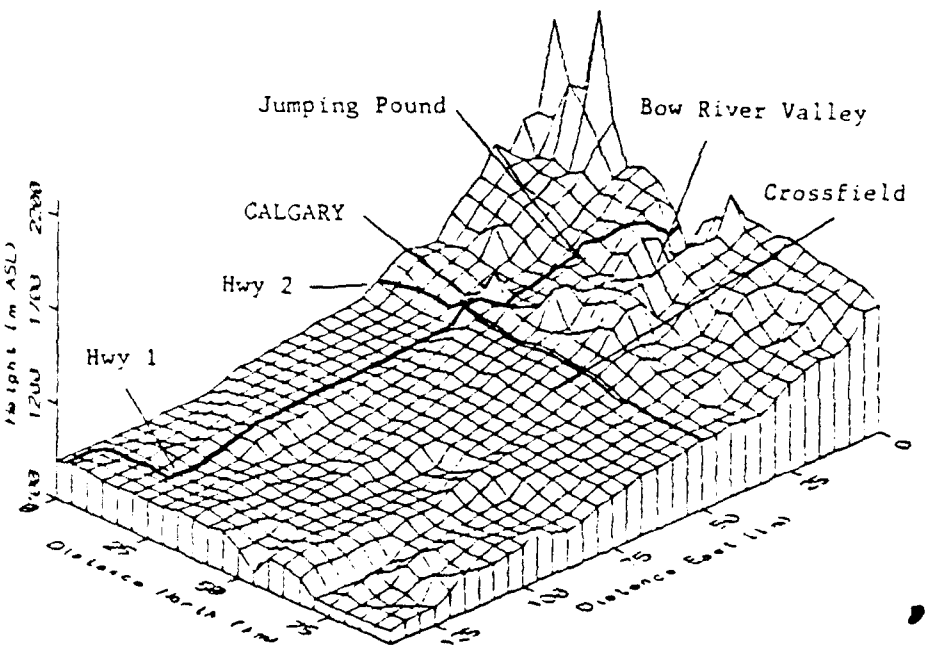

Figure 8. Three-dimensional perspective of model terrain for the computational domain in Calgary area. The view is toward the southwest.

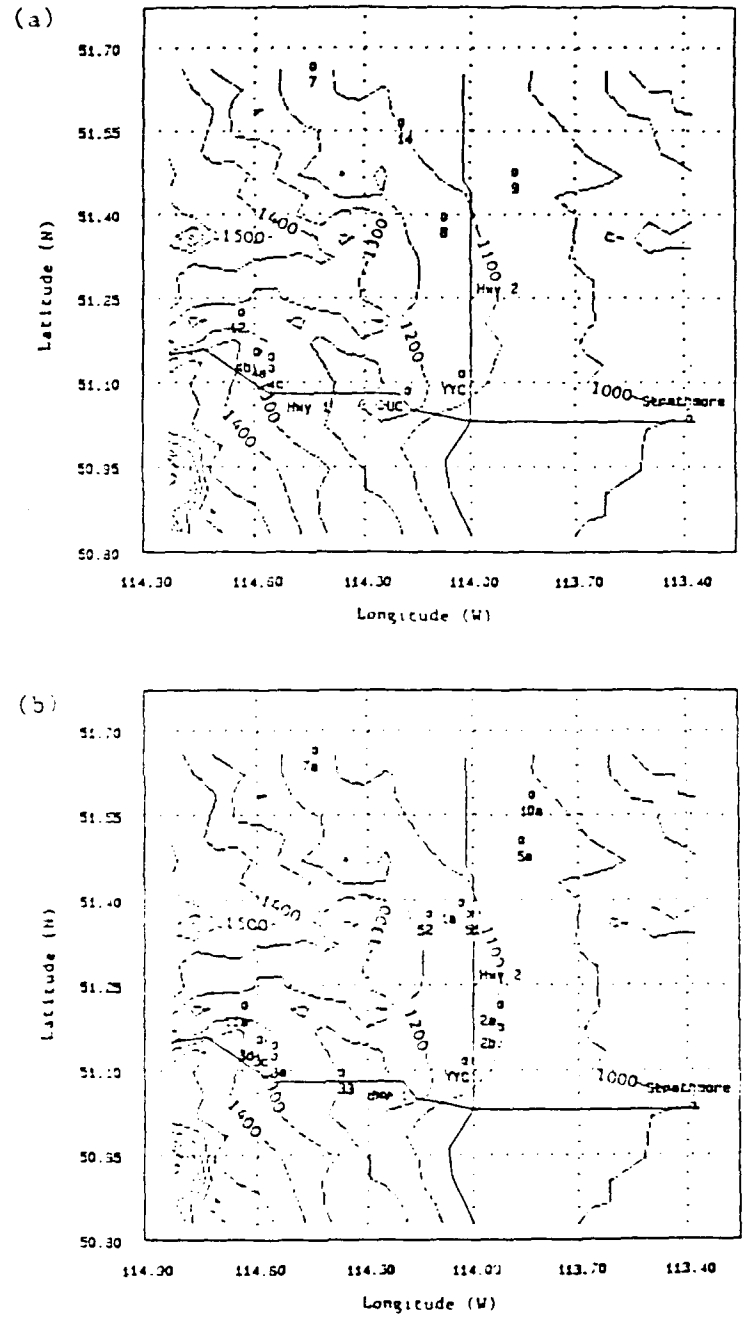

Figure 9. Model grid domain and surface stations for (a) 3 November 1975 and (b) 27 March 1986 cases. Dotted lines are contours of terrain height ASL drawn at 100 m intervals.

Table 1. Surface wind stations

(a) 3 November 1975 case

Station Name (Symbol)	Latitude(N)	Longitude(W)
E. Crossfield (8)	51.40	114.07
Carstairs (14)	51.57	114.19
Lone Pine Creek (9)	51.48	113.87
Harmattan (7)	51.67	114.44
Wildcat Hills (12)	51.23	114.63
Jumping Pound NE (4a)	51.15	114.55
Jumping Pound NW (4b)	51.16	114.59
Jumping Pound SE (4c)	51.13	114.55
Univ. of Calgary (UC)	51.09	114.17
Calgary Intl Airport (YYC)	51.12	114.02

(b) 27 March 1986 case

Station Name (Symbol)	Latitude(N)	Longitude(W)
Calgary Intl A.(YYC)	51.12	114.02
Crossfield #2 (2a)	51.22	113.92
Crossfield #3 (2b)	51.13	113.92
Crossfield #4 trailer (1a)	51.40	114.03
E. Crossfield (51)	51.38	114.01
W. Crossfield (52)	51.38	114.12
Jumping Pound NE (3c)	51.15	114.55
Jumping Pound NW (3d)	51.16	114.59
Jumping Pound SE (3e)	51.13	114.55
Lone Pine Creek (10a)	51.59	113.83
Lone Pine Creek S. (5a)	51.51	113.86
Springbank A. (33)	51.10	114.37
Harmattan (7a)	51.67	114.44
Wildcat Hills (11a)	51.22	114.63

Observations of hourly averaged surface winds are shown in Figs. 10-13 for the two cases. Summaries of surface and 700 mb wind observations are presented in Table 2. As noted in the previous section, synoptic patterns for the two storms are similar, however, there are significant differences in the wind distributions. Inspections of plotted and tabulated winds in Figs. 10-13 and Table 2 show that in the 3 November 1975 case, the 700 mb wind speeds are about 25% higher than in the 27 March 1986 case, yet the observed surface winds are higher in the latter case. this difference is more apparent when only surface wind speeds from those stations common to both cases are compared (Table 2). for example, at 1400 MST, the root mean square wind speed for those stations is 16.3 ms^{-1} for the 1975 case and 19.2 ms^{-1} for the 1986 case. In terms of kinetic energy of the observed winds, the latter case is nearly 40% stronger.

(2) Model Sensitivity Tests

An area of great uncertainty in the application of COMPLEX to SDW flow is the relationship of the lowest model flow surfaces to the terrain. For situations in which the flow surfaces intersect terrain, flow proceeds around terrain obstacles rather than over them. One problem is that the degree to which this intersection occurs cannot be determined from the observational data.

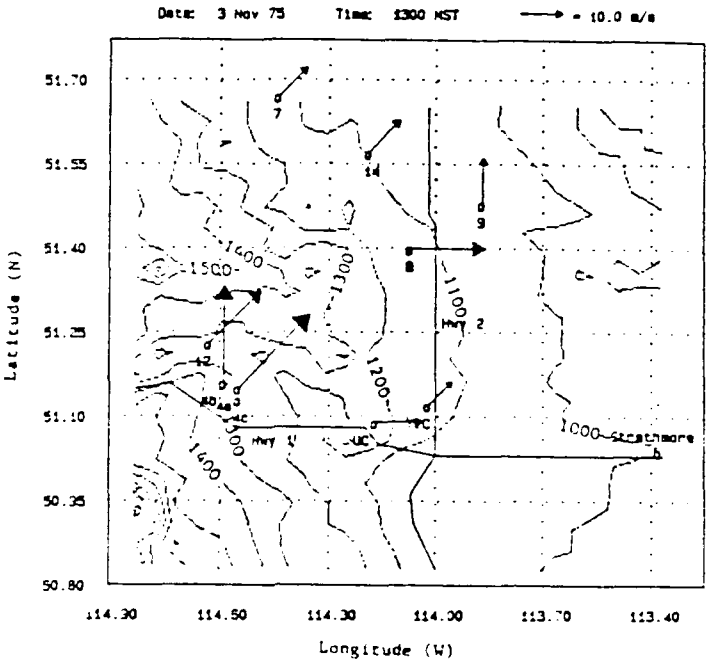

Figure 10. Observed surface winds for 3 November 1975 at 1300 MST. Stations without wind vectors indicate data were not availale for that particular hour.

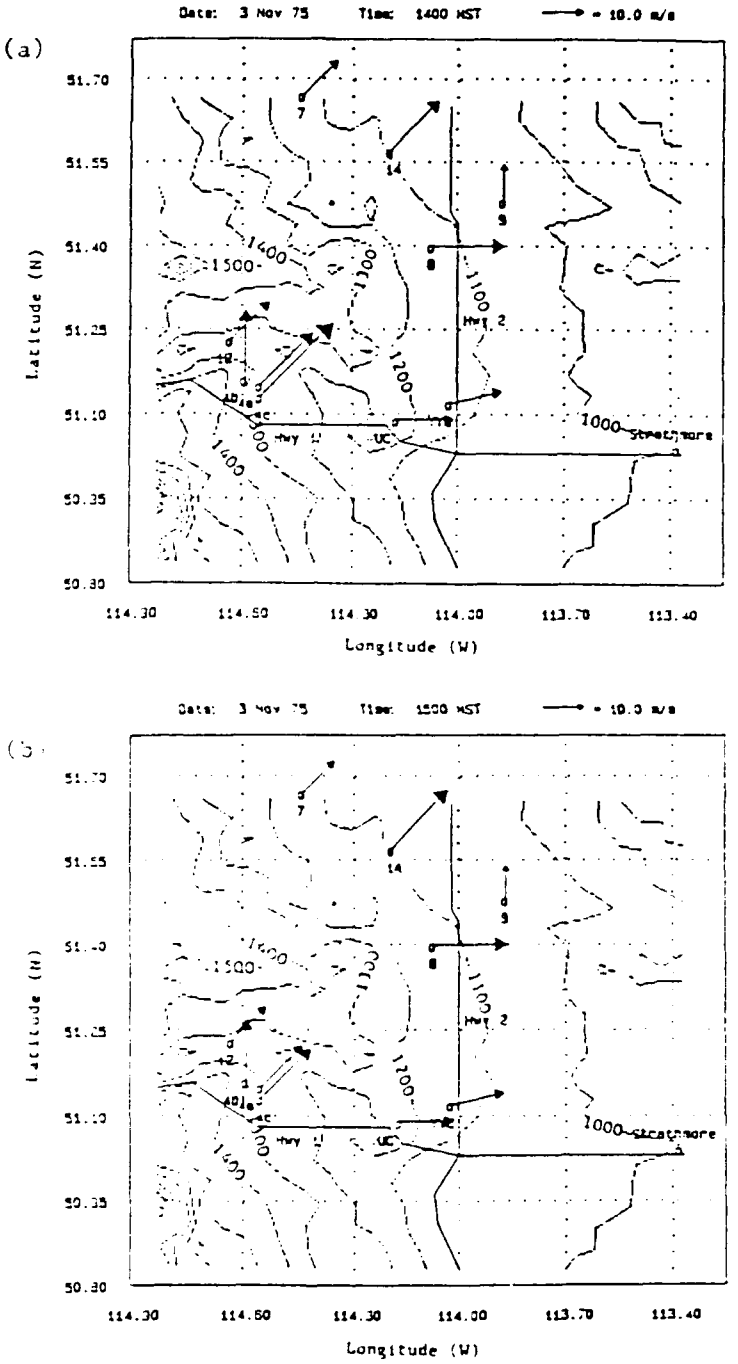

Figure 11. Same as Fig. 10, except for (a) 1400 MST and (b) 1500 MST.

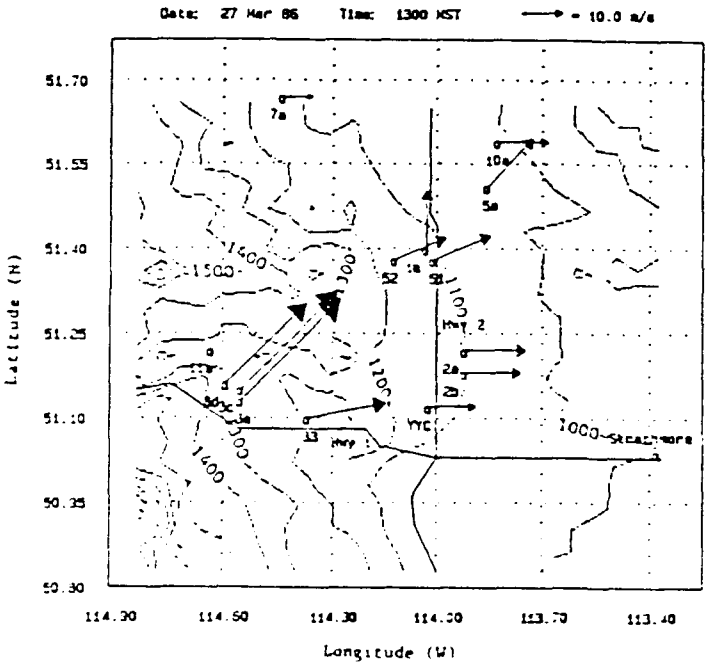

Figure 12. Observed surface winds for 27 March 1986 at 1300 MST. Stations without wind vectors indicate data was not available for that particular hour.

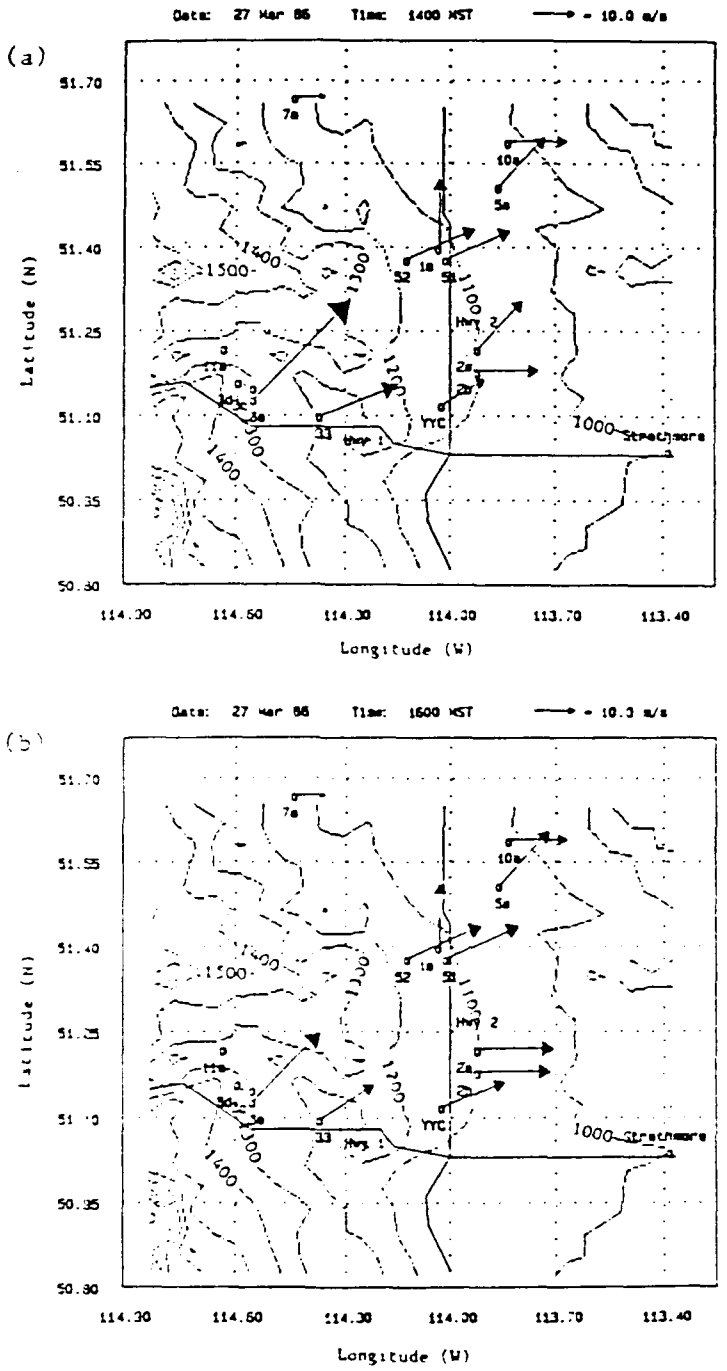

Figure 13. Same as Fig. 12, except for (a) 1400 MST and (b) 1600 MST.

Table 2. Observed surface and 700 mb geostrophic wind speeds and directions.

(a) 3 November 1975

	Wind direction(deg)/speed(m s^{-1})		
	1300 MST	1400 MST	1500 MST
700 mb geostrophic wind	269/25.0	268/25.0	269/25.0
Station Name (Symbol)			
E. Crossfield (8)	270/18.3	270/17.8	270/17.8
Carstairs (14)	225/11.1	225/17.4	225/20.1
Lone Pine Creek (9)	180/11.1	180/8.9	180/8.0
Harmattan (7)	225/9.8	225/12.0	225/10.7
Wildcat Hills (12)	225/17.8	225/12.9	225/11.6
Jumping Pound NE (4a)	225/25.0	225/17.8	225/13.8
Jumping Pound NW (4b)	180/23.2	180/16.5	180/14.3
Jumping Pound SE (4c)	N/A	225/25.0	225/16.5
Univ. of Calgary (UC)	270/12.0	270/14.3	270/13.4
Calgary Intl Airport (YYC)	225/8.0	258/12.9	258/12.9

(b) 27 March 1986

	Wind direction(deg)/speed(m s^{-1})		
	1300 MST	1400 MST	1500 MST
700 mb geostrophic wind	266/18.6	267/18.7	269/18.9
Station Name (Symbol)			
Jumping Pound NE (3c)	225/33.6	N/A	N/A
Jumping Pound NW (3d)	225/27.5	N/A	N/A
Jumping Pound SE (3e)	225/34.7	225/33.6	225/22.5
Lone Pine Creek (10a)	270/13.0	270/14.4	270/14.4
Crossfield #2 (2a)	270/15.2	225/16.1	270/13.8
Crossfield #3 (2b)	270/13.8	270/15.2	270/13.0
Crossfield #4 trailer (1a)	180/13.8	180/16.3	180/15.0
Lone Pine Creek S. (5a)	225/16.6	225/16.6	225/13.0
Calgary Intl Airport (YYC)	270/11.3	240/11.9	250/16.3
E. Crossfield (51)	247/15.2	247/17.5	247/19.7
W. Crossfield (52)	247/13.8	247/18.3	247/20.0
Springbank Airport (33)	260/20.5	250/20.5	240/15.5
Harmattan (7a)	270/6.9	270/6.9	270/6.9
Wildcat Hills (11a)	N/A	N/A	N/A

In the formulation of the flow surface configuration (Eqns. 10-14), the thicknesses between the model flow surfaces and the terrain surface are primarily controlled by the average boundary layer thickness, Z, and the exponential constant, b (Eqn. (12)), so model sensitivity experiments were performed to test both the effect of varying layer thicknesses (Sensitivity tests #1, #2, and #3) and varying wavelength (Sensitivity tests #4, and #5) for the time when the windstorm was at JPd. The 27 March 1986 case was selected for the tests because it contains the most surface wind observations.

An additional problem arose in the formulation of the flow surface configuration. Because the wave trough is forced to progress eastward without changing its shape, the flow surfaces rise as much as 600 m (over 50% of the average boundary layer thickness) near the base of the terrain slope. This behavior does not agree with observations (e.g., Lilly and Zipser, 1972). In order to present a more realistic surface wind field upstream of the wave trough, Ludwig (1987) suggested that the wave shape be modified for cases in which the wave trough is located through Btw and YYC. As a first approximation, the value of b upstream of the wave trough was adjusted so that no change in flow surface height occurred at the southeast corner (anchor point) of the grid as the wave trough was progressed eastward toward Btw and YYC.

Table 3 lists function parameters held constant for all runs, and their values. Values of parameters that were changed for sensitivity tests #1-#5 are listed in Table 4.

Final analyses of the surface wind fields with COMPLEX were accomplished for each case at three separate times: (i) when the windstorm was located at JPd (Fig. 3), (ii) when the storm reached a point midway between JPd and YYC (Btw), and (iii) when it reached YYC. In subsequent sections, these analyses will be referred to as Runs #1, #2, and #3, respectively. As described earlier, the movement of the windstorm was simulated by placing the wave trough axis parallel to the Continental Divide and through each location noted above. The space-time analyses of hourly averaged wind speed shown in Figs. 5 and 7 were used to approximate the time at which the windstorm arrived at those locations.

Table 3. Mountain wave flow parameters held constant for all model runs. Values were derived from Lilly and Zipser (1972) potential temperature analysis of 11 January 1972 Boulder windstorm.

Parameter	Value
Z_{top}	1270 m
Z_{base}	762 m
h_{top}	2134 m
h_{base}	1219 m

Table 4. Mountain wave parameters specified in model sensitivity tests

Sensitivity Test No.	Effective Wavelength (km)	Parameter b (km^{-2})	Z (m)
1.	75.	.0018	1270.
2.	75.	.0018	1000.
3.	75.	.0018	1100.
4.	50.	.0044	1100.
5.	100	.0011	1100.

Chapter 4

RESULTS

a. Sensitivity Tests

(1) Effect of Boundary Layer Thickness

In tests #1, #2, and #3, the value of b in Eqn. 16 was set to produce an effective wavelength of 75 km and the boundary layer thickness was systematically varied. East-west cross sections of the model flow surfaces and the terrain surface through JPd and YYC are presented in Fig. 14 for tests #1 and #2. The respective surface wind vectors and isotach analyses are shown in Figs. 15 and 16. In each analysis, the wave trough axis is represented by a heavy dashed line. For clarity, surface wind vectors are displayed at 8.338 km intervals (odd numbered rows and columns). Isotachs are plotted at a 5 m s^{-1} intervals and areas of wind speeds exceeding 15 m s^{-1} are cross-hatched.

In test #1 Z was set equal to Z_{top} (1270 m) to determine the effect of allowing the flow surfaces to intersect the terrain. Wind vectors in Figure 15 indicate flow is increased near the wave trough axis, particularly through the Bow River Valley near Wildcat Hills (station 11a) where westerly wind speeds exceed 25 m s^{-1}. The largest gradients in wind direction are noted in the Bow River Valley and along the northern, western, and southern boundaries. A speed minimum ($\leq$ 10 m s^{-1}) is found over the hilltops near

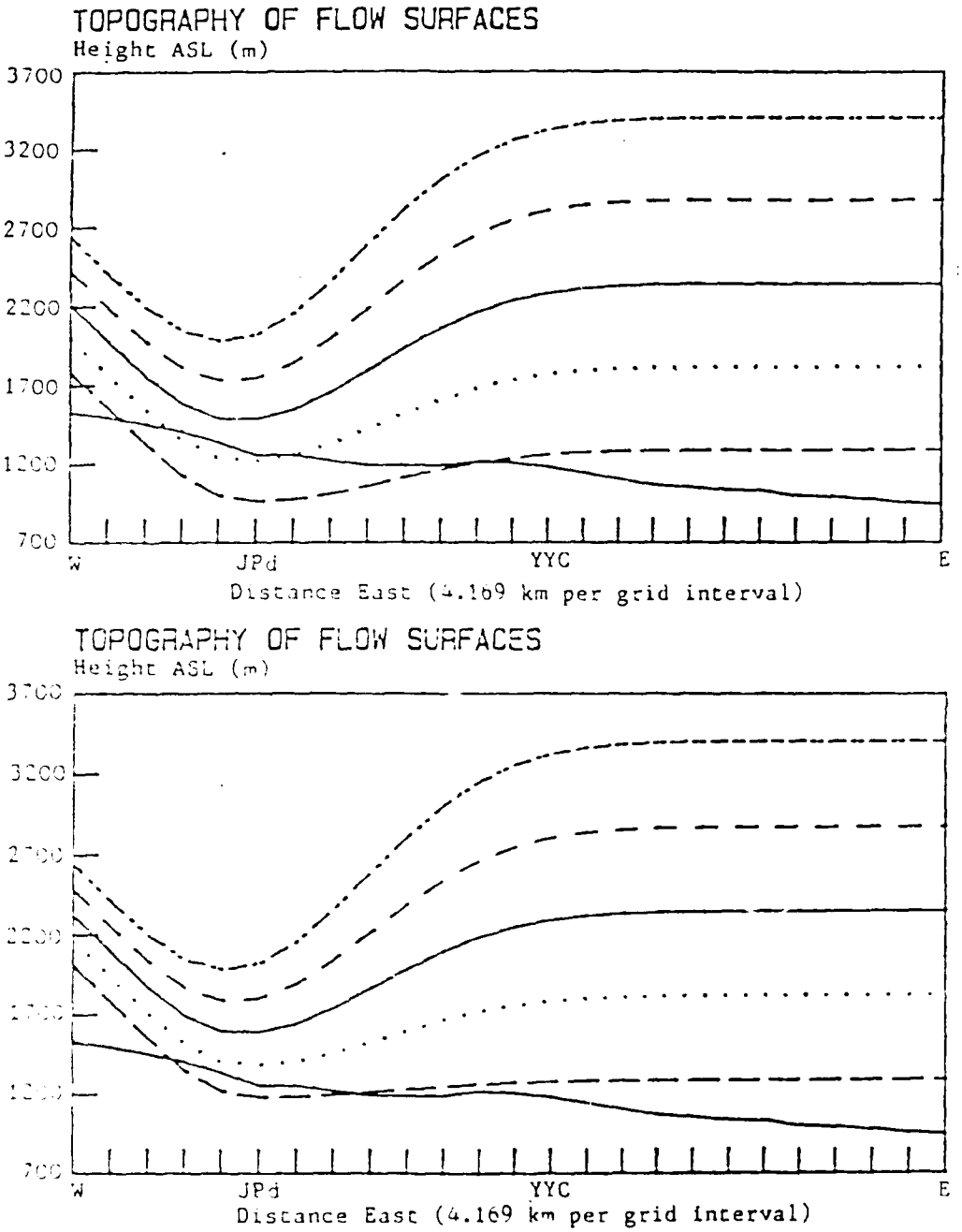

Figure 14. East-west vertical cross section through Jumping Pound (JPd) and Calgary International Airport (YYC) of model flow surfaces for (a) Sensitivity test #1 and (b) Sensitivity test #2. Lines from bottom to top are the terrain surface and the five upper model flow surfaces. Note: Sensitivity test #3 produced optimum results. The corresponding cross section is presented just prior to the case studies (Figure 22).

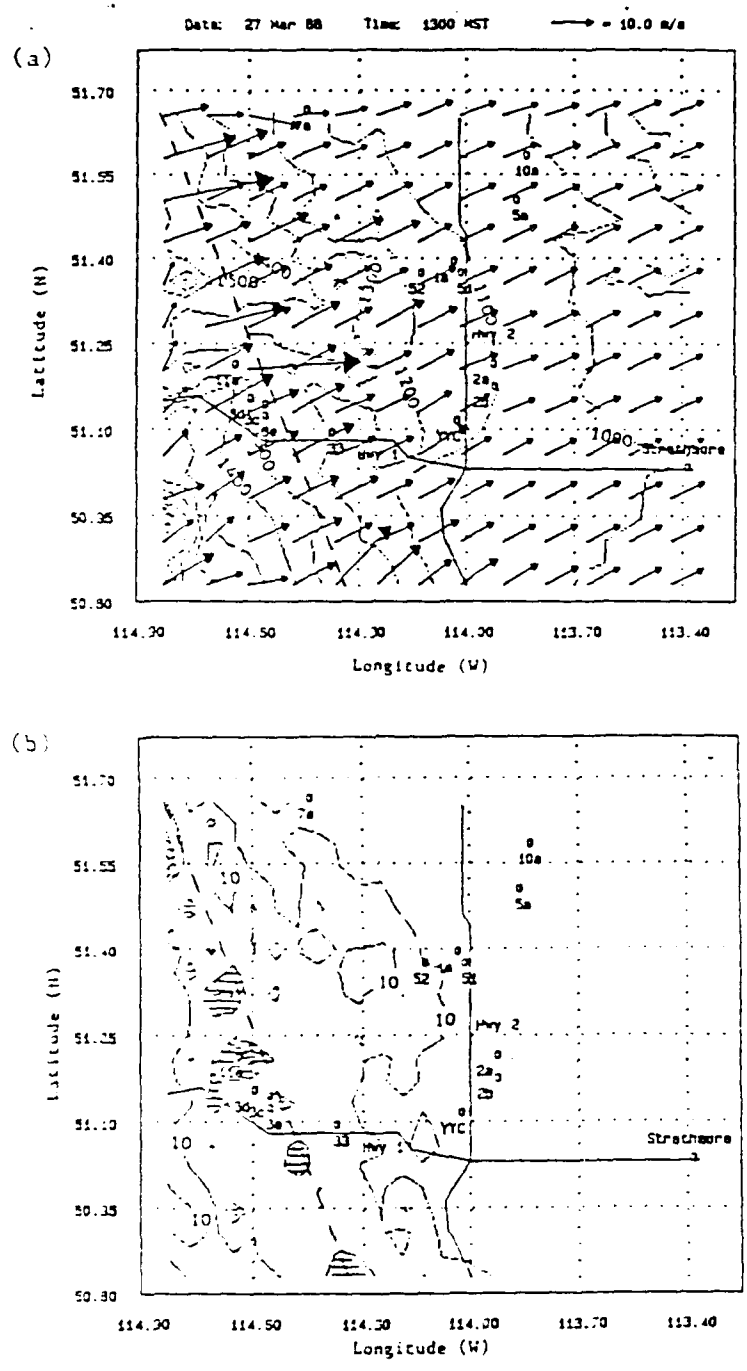

Figure 13. Model anemometer height (a) wind vectors and (b) isotach analysis for Sensitivity test #1. In (b), isotachs are drawn at 5 m/s intervals and winds exceeding 15 m/s are indicated by cross hatching. The wave trough axis is indicated by a dashed line.

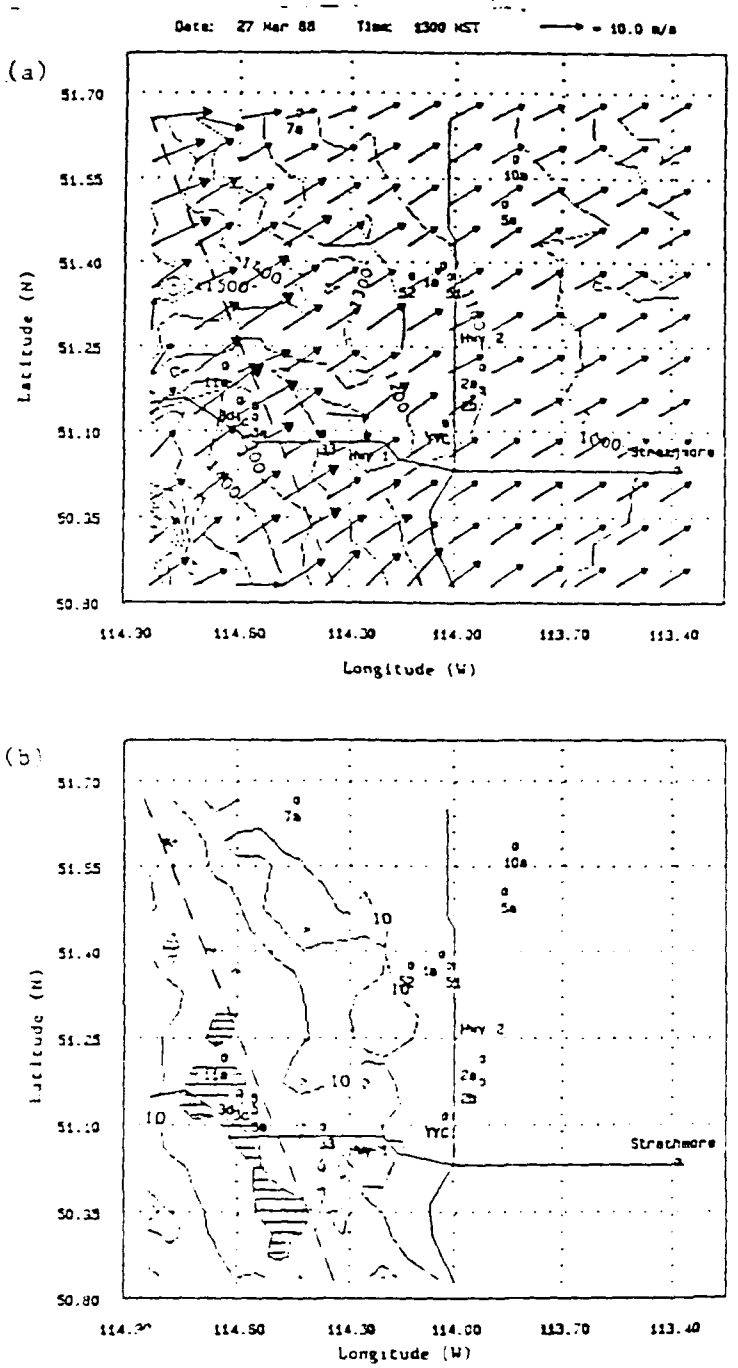

Figure 16. Same as Fig. 15, except for Sensitivity test #2.

51.40N, 114.30W while wind speeds exceeding 10 m s^{-1} occur between that location and Highway 2 to the east.

In general, test #1 shows several realistic results due to both mesoscale forcing and topography: (i) increased winds are near the wave trough, (ii) WSW wind directions with small scale variations due to terrain features, and (iii) numerous wind speed maxima/minima which reflect terrain details. However, model wind speeds substantially underestimate observed wind speed values (Fig. 10, Table 2) at JPd (stations 3c, 3d, and 3e), Springbank Airport (station 33), and W. Crossfield (station 52) by 30-75% (4-21 ms^{-1}).

In test #2, Z was reduced to 1000 m to reduce the degree of terrain intersection of the flow surfaces at the base of the terrain slope. Patterns of model winds relative to wave trough location are similar to those produced in test #1 (Fig. 15) except that fewer winds exceed 20 m s^{-1}, and there is a larger area of winds exceeding 15 m s^{-1} along the wave trough axis near JPd. Wind direction varies little through the grid domain except at the boundaries and over the hills just west of Crossfield #2 (Station 2a). Model wind speeds near JPd (17 m s^{-1}) and Springbank (12 m s^{-1}) are closer to the observed values then in test #1. Greater wind speeds also occur at the base of the mountains near the southwest grid corner. Problems still exist near W. Crossfield where the model wind speed underestimates the observed

wind speed even more than in test #1, and the maximum model wind speed severely underestimates observed maximum wind speed (20 vs 34 m s^{-1}).

In test #3, Z was set to 1100 m, i.e., an intermediate value between tests #1 and #2. This test produced the best results. The west-east distribution of model wind speed through JPd, Springbank Airport (Spr), and YYC are shown in Fig. 17 for tests #1, #2, and #3. Variation in wind speed response to terrain from test-to-test is apparent, as from Spr to YYC wind speed increases and decreases do not occur at the same terrain points. Near JPd, all three tests produce wind speed maxima, but only in test #3 is the maximum model wind speed (30 ms^{-1}) close to the observed value (34 m s^{-1}).

(2) Effect of Lee Wave Length

In tests #4 and #5, the value of Z was fixed at 1100 m while the value of b was varied to produce effective wavelengths of 50 km and 100 km, respectively. East-west cross sections of the model flow surfaces through JPd and YYC are presented for both tests in Fig. 18. The respective surface wind vectors and isotach analyses are presented in Figs. 19 and 20.

In test #4 (Fig. 19), the relatively short wavelength produces a narrow region of increased surface wind flow. Wind speed maxima ($\geq$ 20 m s^{-1}) occur in line with the wave trough axis. Maximum model wind speeds (27 m s^{-1}) occurs

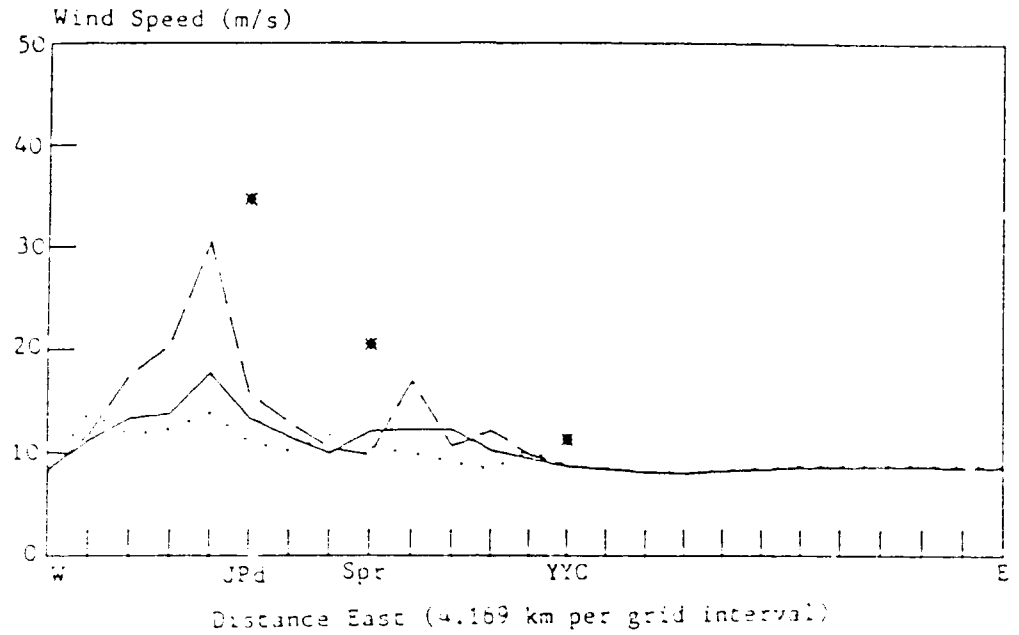

Figure 1'. East-west variation of model anemometer height wind speed through Jumping Pound (JPd), Springbank (Spr), and Calgary International Airport (YYC) for Sensitivity tests #1, #2, and #3. Observed wind speeds are denoted by an asterisk while dotted, solid, and dashed lines represent tests #1, #2, and #3, respectively.

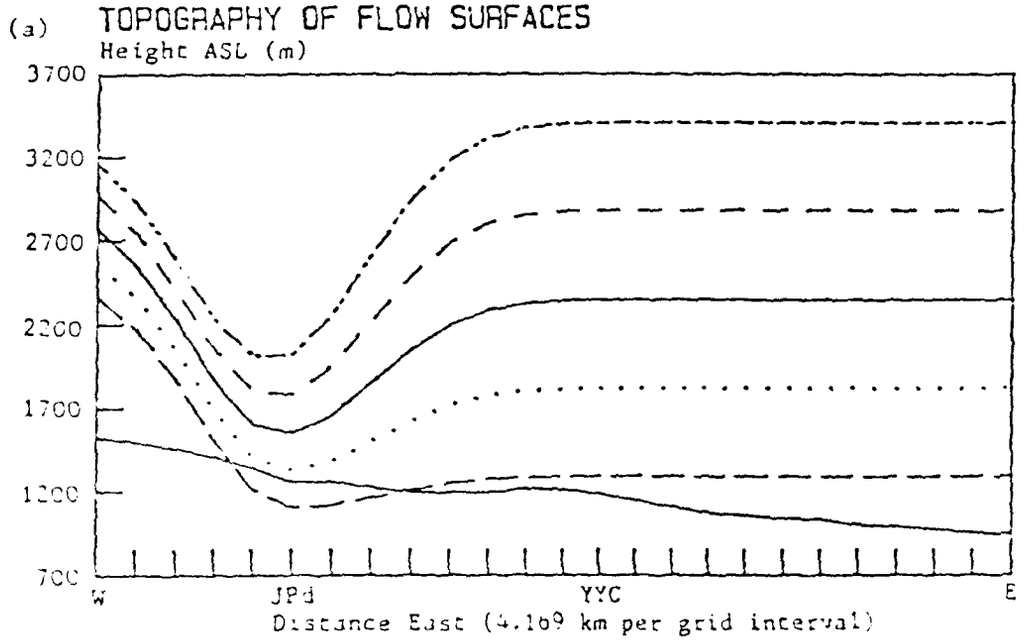

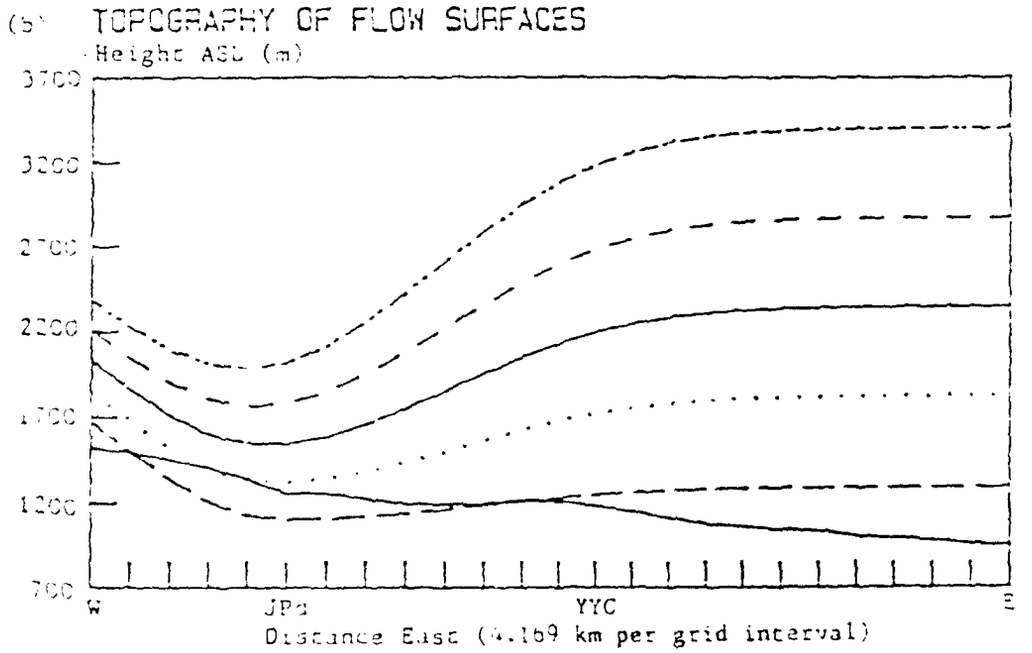

Figure 18. Same as Fig. 14, except for (a) Sensitivity test #4 and (b Sensitivity test #5.

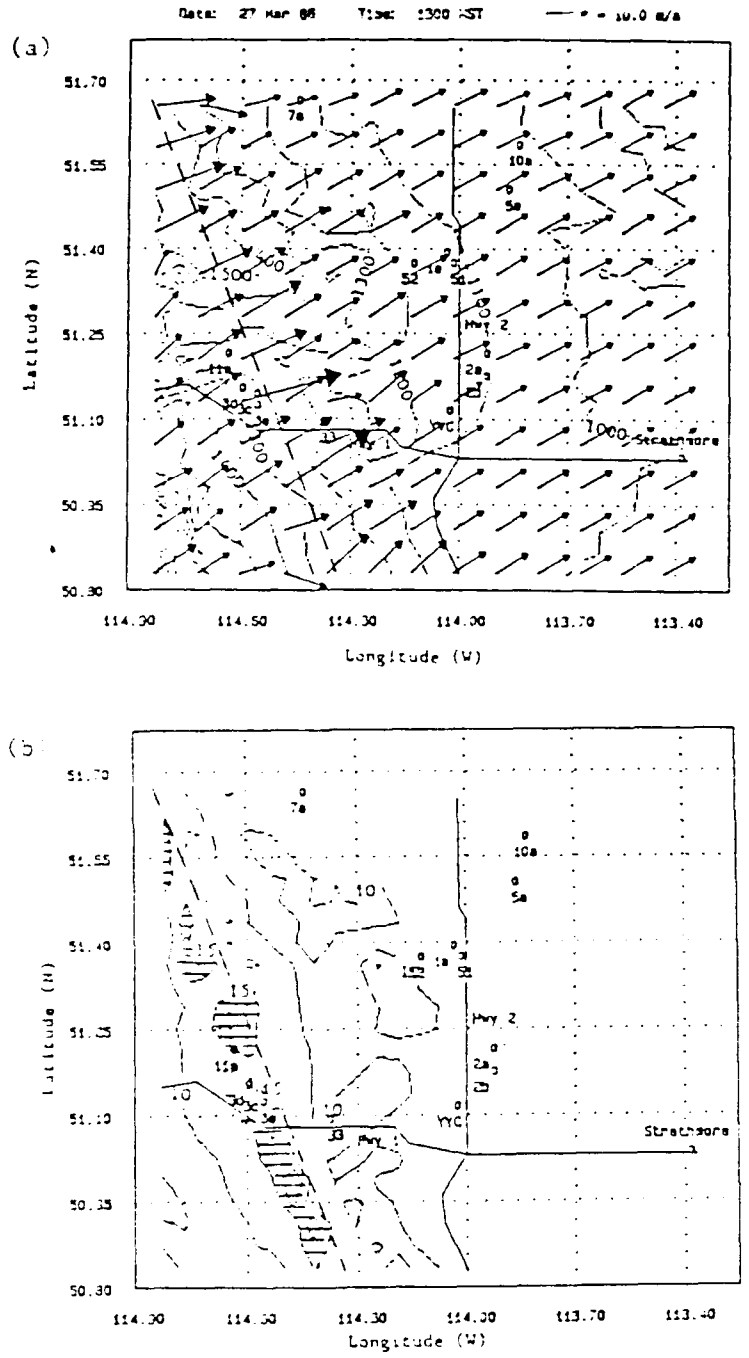

Figure 19. Same as Fig. 15, except for Sensitivity test #4.

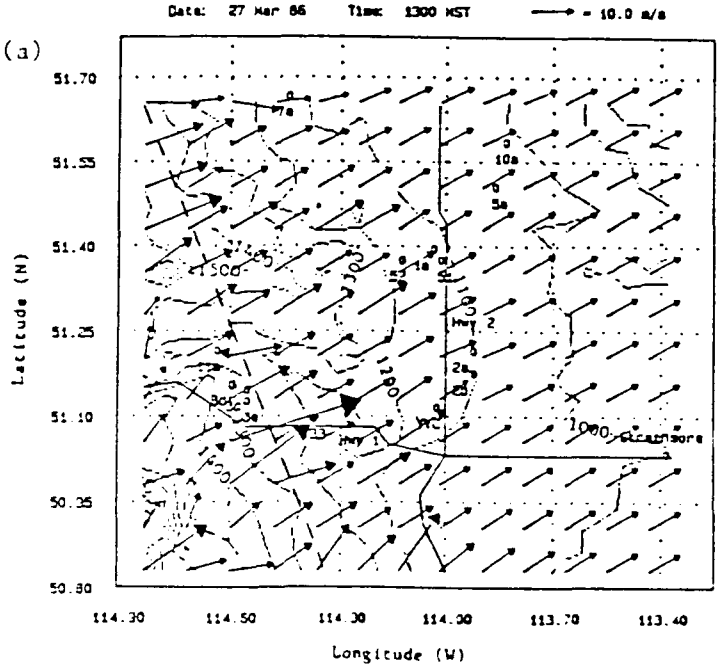

Figure 20. Same as Fig. 15, except for Sensitivity test #5.

near 51.25N, 114.70W. Downstream of the wave trough, wind speed and direction show small gradients. Only slight variations in wind direction occur near JPd, while greater wind shifts occur along the lateral boundaries.

Several poor results were noted in test #4. These included: (i) maximum model wind speed (27 m s^{-1}) are less than 80% of the observed value (34 m s^{-1}); (ii) model wind speeds underestimate observed values at JPd, Springbank, and W. Crossfield; and (iii) little model response to terrain features. Only near the wave trough axis do the model wind vectors appear to respond realistically to terrain variations.

The longer wavelength in test #5 (Fig. 20), produces increased model wind speeds downstream of the wave trough axis. Patterns of wind speed maxima/minima similar to Fig. 15 are produced, except that high winds occur south of JPd. Maximum model wind speeds (33 m s-1) are found at 51.05N, 114.60W. In addition, more realistic variations in wind direction occur in the Bow River Valley near Wildcat Hills and down the steep slope from the southwest corner of the grid.

Generally, test #5 shows that an increase in the horizontal scale of mesoscale forcing causes an increase of the horizontal extent of strong surface winds. In addition, the maximum model wind speed is comparable to the observed value (33 vs 34 m s^{-1}) and model winds are more responsive to

terrain features. However, some of the problems in other tests also occur in test #5. Observed speeds near JPd, Springbank, and W. Crossfield are significantly underestimated.

In an effort to position the wind speed maximum closer to JPd, the value of b was adjusted to produce an effective wavelength of 75 km with Z set at 1100 m (Test #3). The west-east distribution or model winds through JPd, Springbank (Spr), and YYC are presented for tests #3, #4, and #5 in Fig. 21. All three tests show increases in wind speed near JPd, but only test #3 produces a model wind speed comparable to the observed value at that location. Thus, the combined results of all tests (Figs. 17, 21) show clearly that test #3 produces the best results.

In the two case studies which are presented in the following section, flow surface parameters (b,Z) defined by sensitivity test #3 are used to represent the windstorm at JPd (Run #1). As the storm "moves eastward," i.e., as the trough is subsequently positioned at Btw (Run #2) and YYC (Run #3), flow surface shapes were modified so that no change in flow surface height occurred at the southwest grid corner. The resulting function parameters for each case run are specified in Table 5 while east-west cross sections of the model flow surfaces through JPd, Btw, and YYC are presented in Figs. 22 and 23.

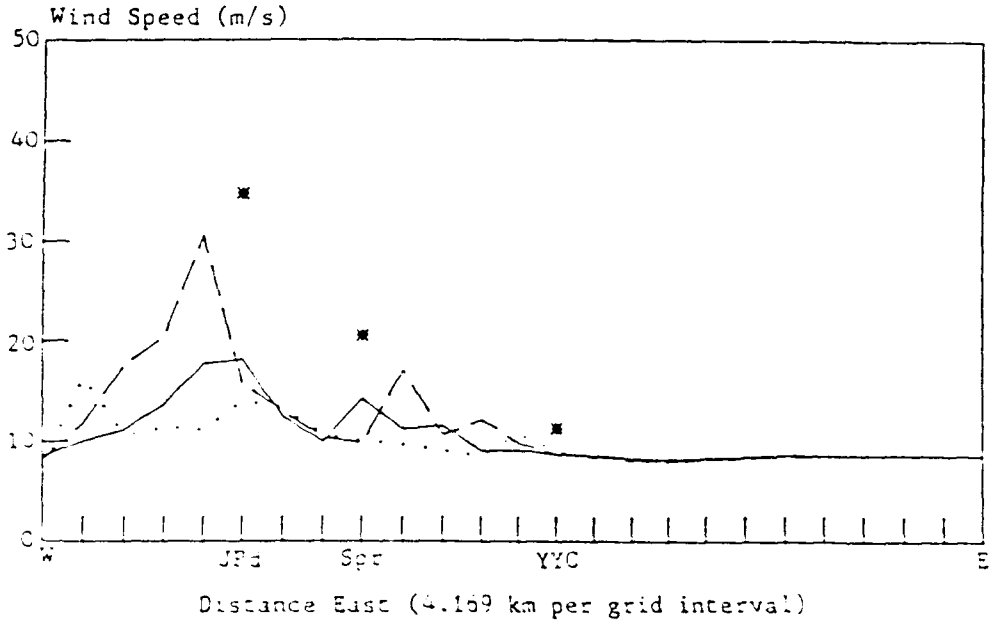

Figure 21. Same as Fig. 17, except for Sensitivity tests #3, #4, and #5. Observed wind speeds are denoted by an asterisk while dashed, solid, and dotted lines represent tests #3, #4, and #5, respectively.

Table 5. Mountain wave flow parameters specified for 3 November 1975 and 27 March 1986 case studies (see Figs. 22 and 23a,b).

		Parameter			
Case Run No.	Wave Position	b[upstream] (10^{-3} km^{-2})	b[downstream] (10^{-3} km^{-2})	Z (m)	Figure
1.	JPd	1.800	1.8	1.1	22
2.	Btw	0.767	1.8	1.1	23a
3.	YYC	0.420	1.8	1.1	23b

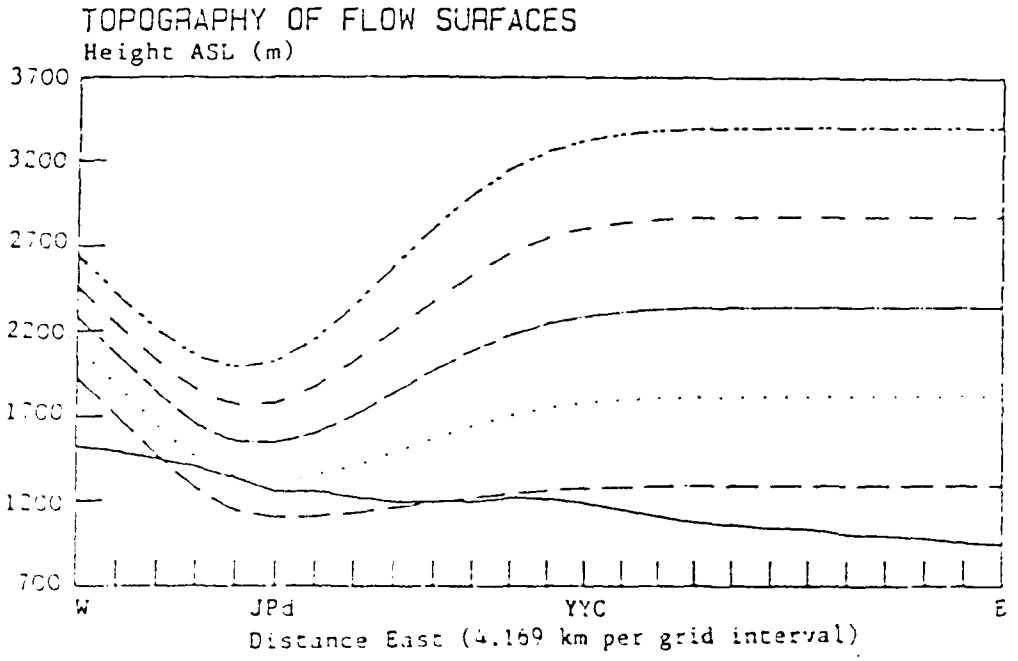

Figure 22. East-west vertical cross section through Jumping Pound (JPd) and Calgary International Airport (YYC) of model flow surfaces for Case Run #1 (Sensitivity test #3). Lines from bottom to top are the terrain surface and the five upper model flow surfaces.

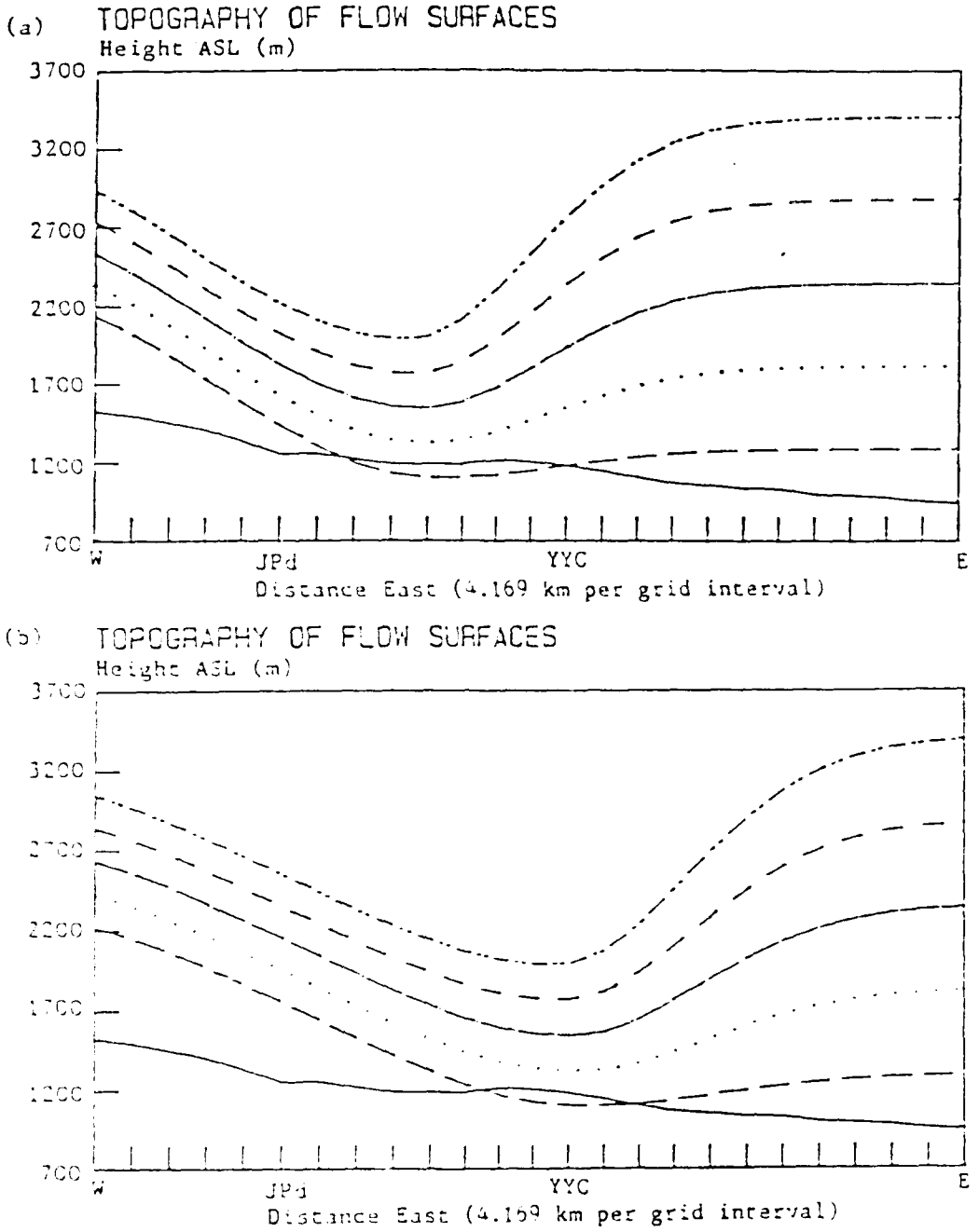

Figure 23. Same as Fig. 22, except for (a) Case Run #2 and (b) Case Run #3.

b. Case Studies

(1) 3 November 1975

Model anemometer height wind vectors and isotach analyses are presented for case runs #1, #2, and #3 in Figs. 24, 25, and 26, respectively. For ease in comparison, these figures are grouped at the end of each case discussion. In this and in the 27 March 1986 case study, the position of the wave trough is indicated by a heavy dashed line and areas of wind speeds exceeding 15 m s^{-1} are indicated by cross-hatching.

On 3 November 1975 the wave trough moved across the western portion of the domain to arrive at JPd at 1300 MST (Fig. 24), Btw at 1400 MST (Fig. 25), and finally YYC at 1500 MST (Fig. 26). As noted in the discussion of Fig. 5. The times are approximate; Lester (1978a) provides some evidence which suggests that the windstorm moved more rapidly as it moved past Calgary.

As expected, the distribution of wind speeds at each time is roughly symmetric with respect to the position of the wave trough. As the wave trough is moved from JPd to YYC, model wind speeds are stronger near the trough. The highest wind speeds and wind speed gradients appear upstream of the trough axis. Downstream , away from the wave trough, wind speeds decrease gradually. Wind directions are mostly SW-WSW with greatest variations along the wave trough near

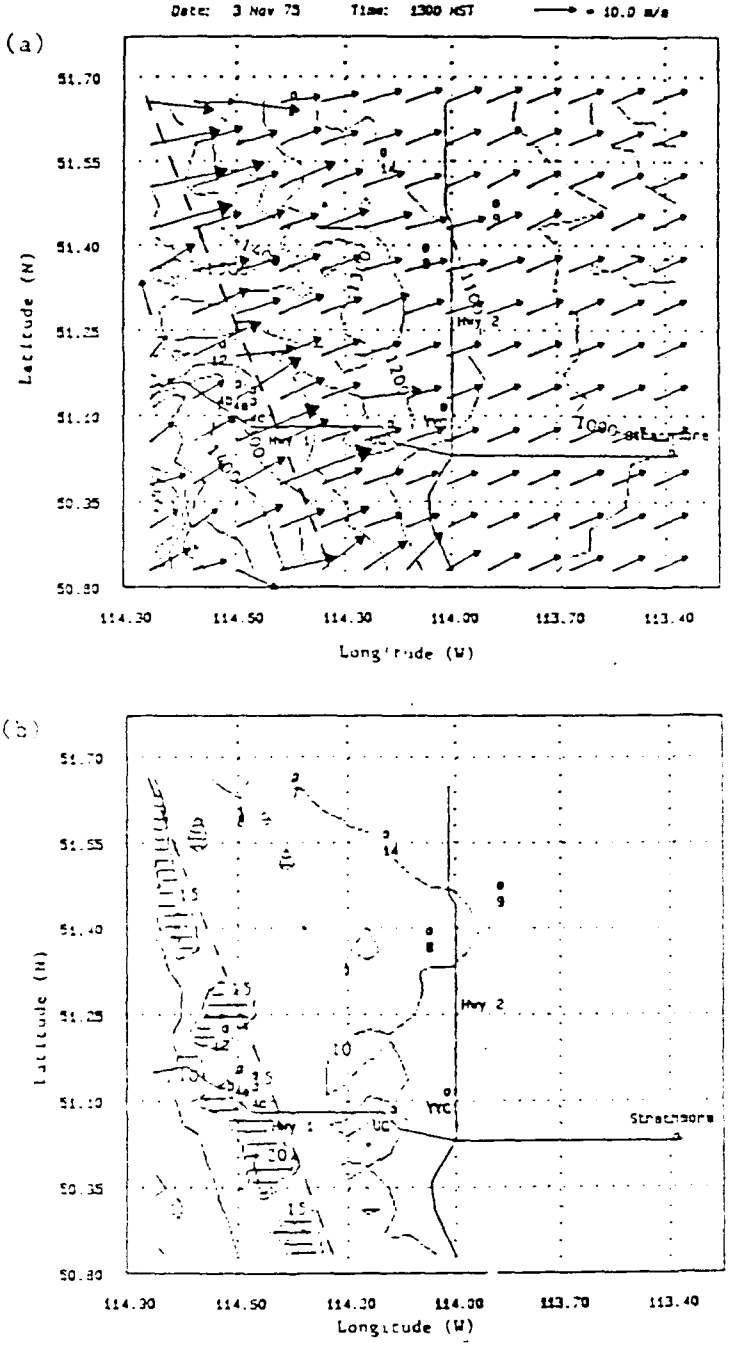

Figure 24. Model anemometer height (a) wind vectors and (b) isotach analysis for 3 November 1975 at 1300 MST (Case Run #1). In (b), isotachs are drawn at 5 m/s intervals and winds exceeding 15 m/s are indicated by cross hatching. The wave trough axis is indicated by a dashed line.

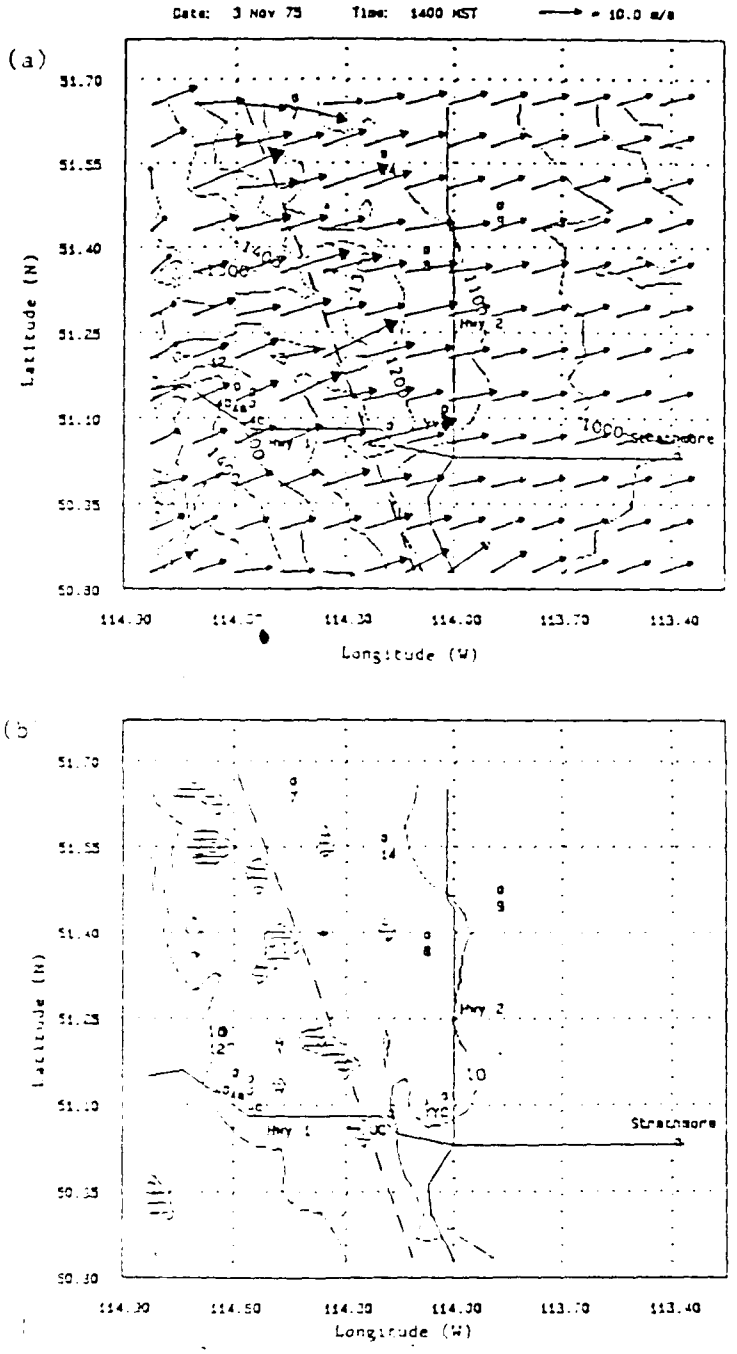

Figure 25. Same as Fig. 24, except for 1400 MST (Case Run #2).

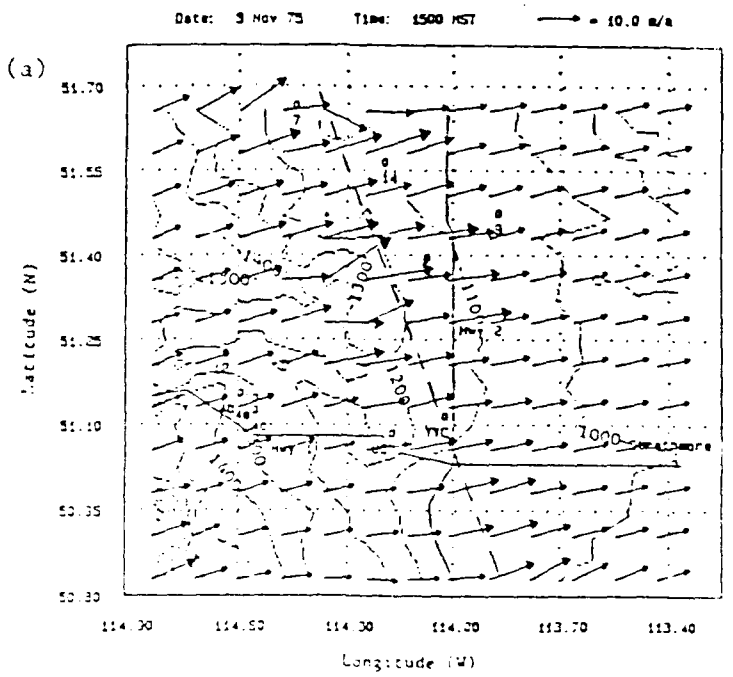

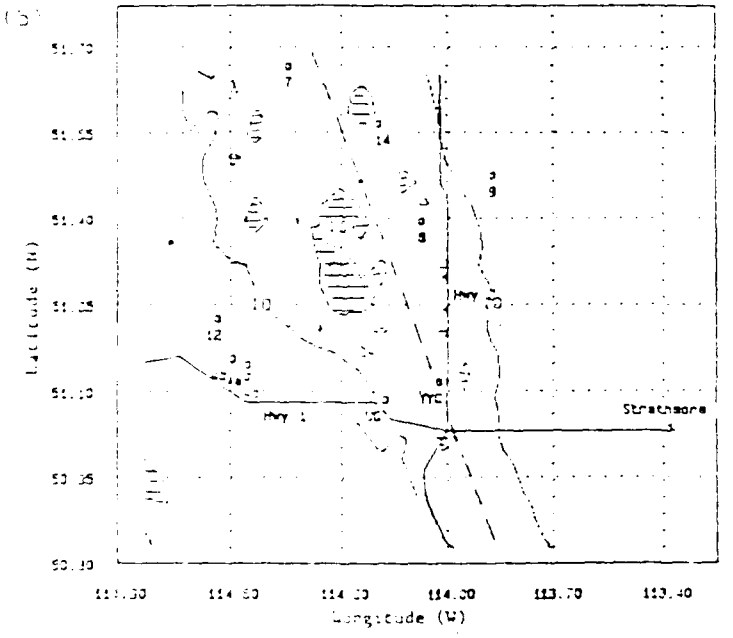

Figure 25. Same as Fig. 24, except for 1500 MST (Case Run #3).

relatively steep terrain features and along the lateral boundaries.

Wind speed maxima and minima are very localized and occur near both local maxima and minima in terrain elevations. This variability is well-illustrated in Figs. 25 and 26. In Fig. 25, a wind speed maximum ($\geq$ 20 m s^{-1}) occurs directly over a terrain peak ($\geq$ 1300 m) at 51.05N, 114.25W with lighter winds in the lower elevations surrounding the peak. Near a higher terrain peak ($\geq$ 1400 m) at 51.22N, 114.25W, wind speed is higher around the peak than it is directly over it. Similarly, in Fig. 26, a wind speed maximum ($\geq$ 25 m s^{-1}) occurs at a relatively lower terrain elevation between two hill tops ($\geq$ 1400 m) at 51.32N, 114.30W with relatively lighter winds directly over the terrain peaks. This may be an artifact that occurs near intersections of a flow surface with the terrain. Adjustment toward non-divergence may lead to unrealistically high speeds in terrain gaps.

The highest model wind speeds occur with the wave positioned through JPd (Fig. 24). The maximum model wind speed (32 m s^{-1}) occurs at 51.37N, 114.50W and 30 m s^{-1} winds appear at 51.10N, 114.50W near JPd (stations 4a, 4b, and 4c).

As the wave trough moved eastward to BtW (Fig. 25), areas of winds exceeding 20 m s^{-1} decrease. Maximum model

wind speed (25 m s^{-1}) with the trough at BTW occurs at 51.17N, 113.31W.

When the wave trough is moved to YYC (Fig. 26), the maximum wind speed (26 m s^{-1}) appears at 51.31N, 114.30W, within a larger area of winds exceeding 15 m s^{-1}. Areas of winds exceeding 20 m s^{-1} have diminished in size and number.

A comparison of case runs #1, #2, and #3 (Figs. 24, 25, and 25) with the respective observed surface winds (Figs. 10, 11a, and 11b) shows that the model successfully reproduces high winds observed at the base of the major terrain slope for the case in which the wave trough is located through JPd. Additionally, model winds near Harmattan (station 7) and Carstairs (station 14) respond realistically, i.e., they increase as the wave trough is moved eastward. Good agreement between model and observed wind speeds is obtained near YYC for all three case runs. Underestimates of observed wind speeds by the model occur at JPd for cases in which the wave trough is located to the east, and at Crossfield (station 8) for all three runs. In each of these situations, the stations are too far away from the wave trough to be affected by the model wave influence. This indicates that the actual flow structure may feature a mountain wave mode whose influence (i.e., mesoscale forcing of boundary layer thickness) is horizontally more extensive than the 'hydrostatic wave' structure specified in Chapter 3.

(2) 27 March 1986

Model anemometer height wind vectors and isotach analyses are presented for case runs #1, #2, and #3 in Figs. 27, 28, and 29, respectively. The wave trough was moved across the western portion of the domain to arrive at JPd at 1300 MST (Fig. 27), Btw at 1400 MST (Fig. 28), and finally YYC at 1600 MST (Fig. 29).

There are several similarities between this case and the 3 November 1975 case. The surface wind speed distribution at each time is symmetric with respect to the position of the wave trough. As the wave trough moves eastward from JPd to YYC, model wind speeds increase near the trough and decrease elsewhere. The highest wind speeds and wind speed gradients appear upstream of the trough axis. Also, flow is mostly SW-WSW with the greatest variations in wind direction along the wave trough near relatively steep terrain features and along the lateral boundaries. Finally, wind speed maxima and minima are very localized, and may occur near either local maxima or minima in terrain elevation.

A difference between this case and the 3 November case appears when the wave is located through both JPd and Btw (Figs. 27 and 28). Secondary wind maxima (> 10 m s^{-1}) appear downstream of the wave trough axis. Model wind speeds decrease below 10 m s^{-1} between 51.15N, 114.30W and 51.65N, 114.60W and increase above 10 m s^{-1} immediately downstream. The boundaries of the secondary maxima appear

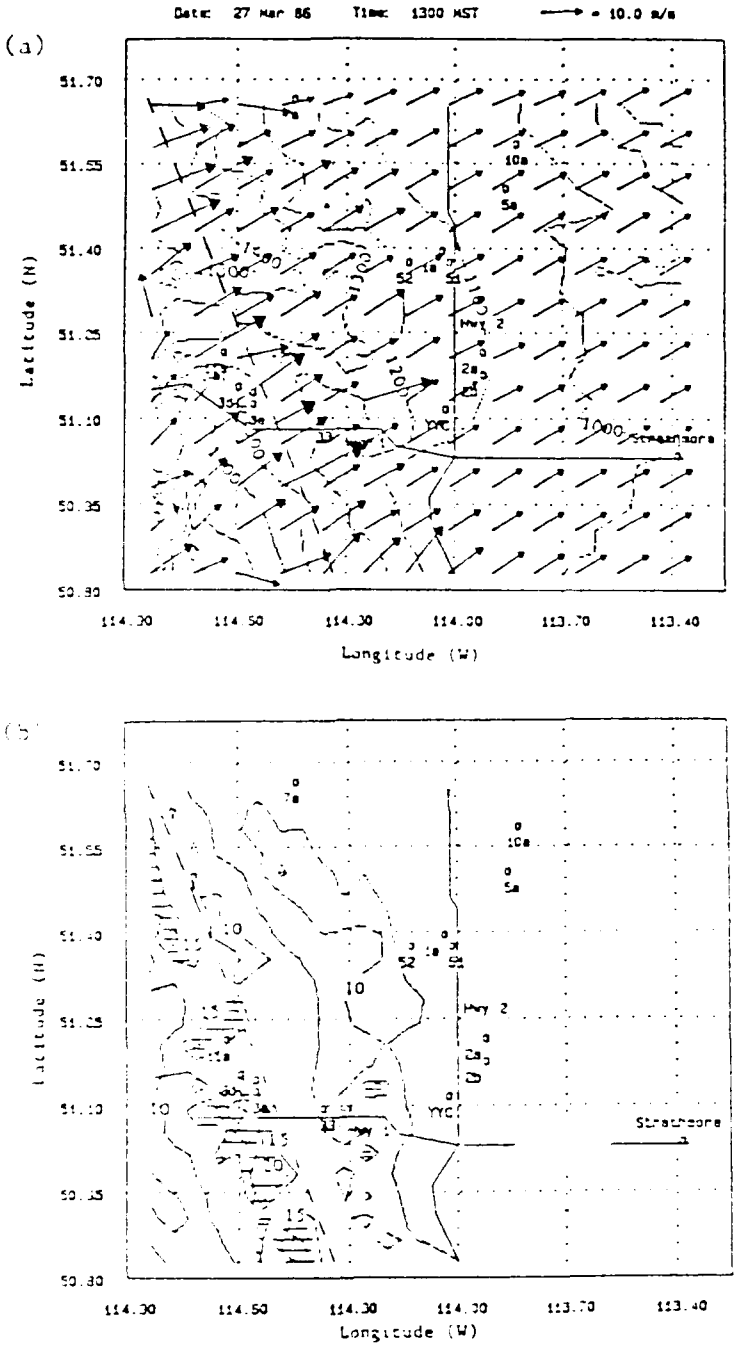

Figure 27. Model anemometer height (a) wind vectors and (b) isotach analysis for 27 March 1986 at 1300 MST (Case Run #1). In (b), isotachs are drawn at 5 m/s intervals and winds exceeding 15 m/s are indicated by cross hatching. The wave trough axis is indicated by a dashed line.

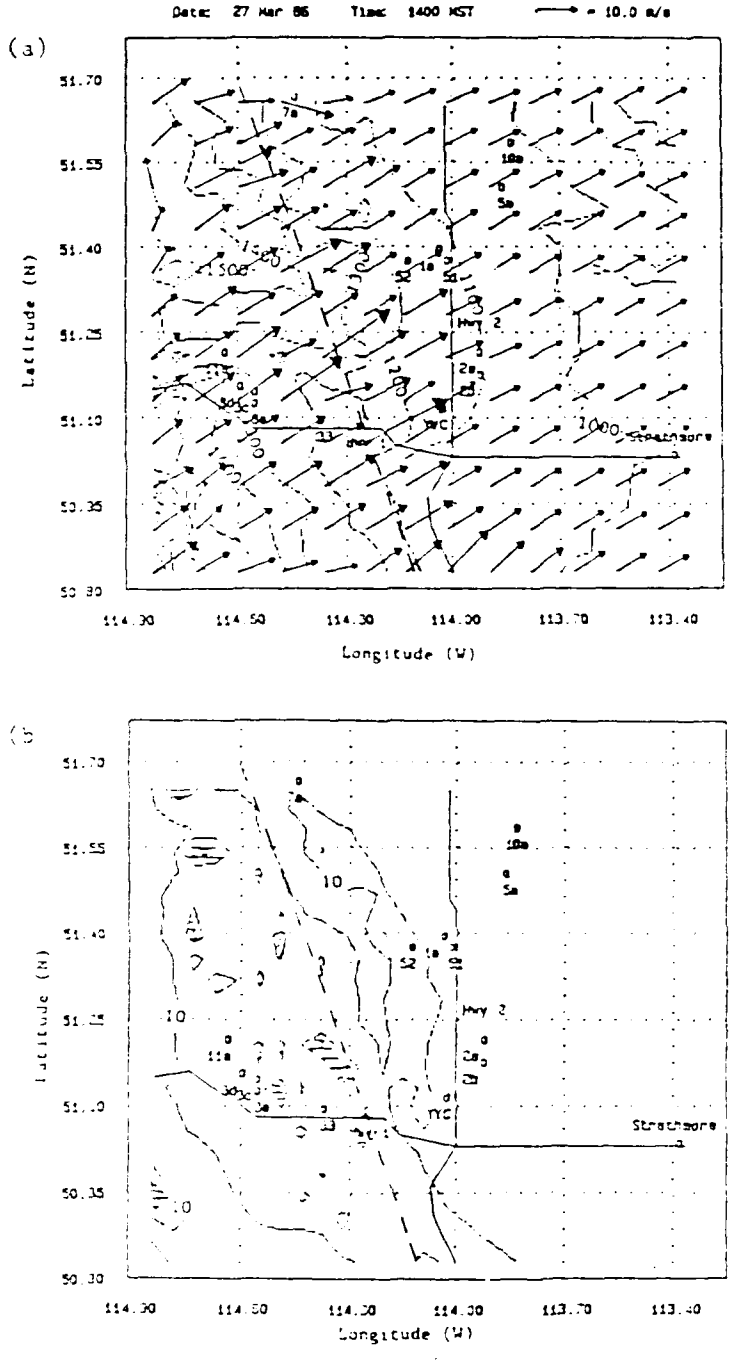

Figure 28. Same as Fig. 27, except for 1400 MST (Case Run #2 .

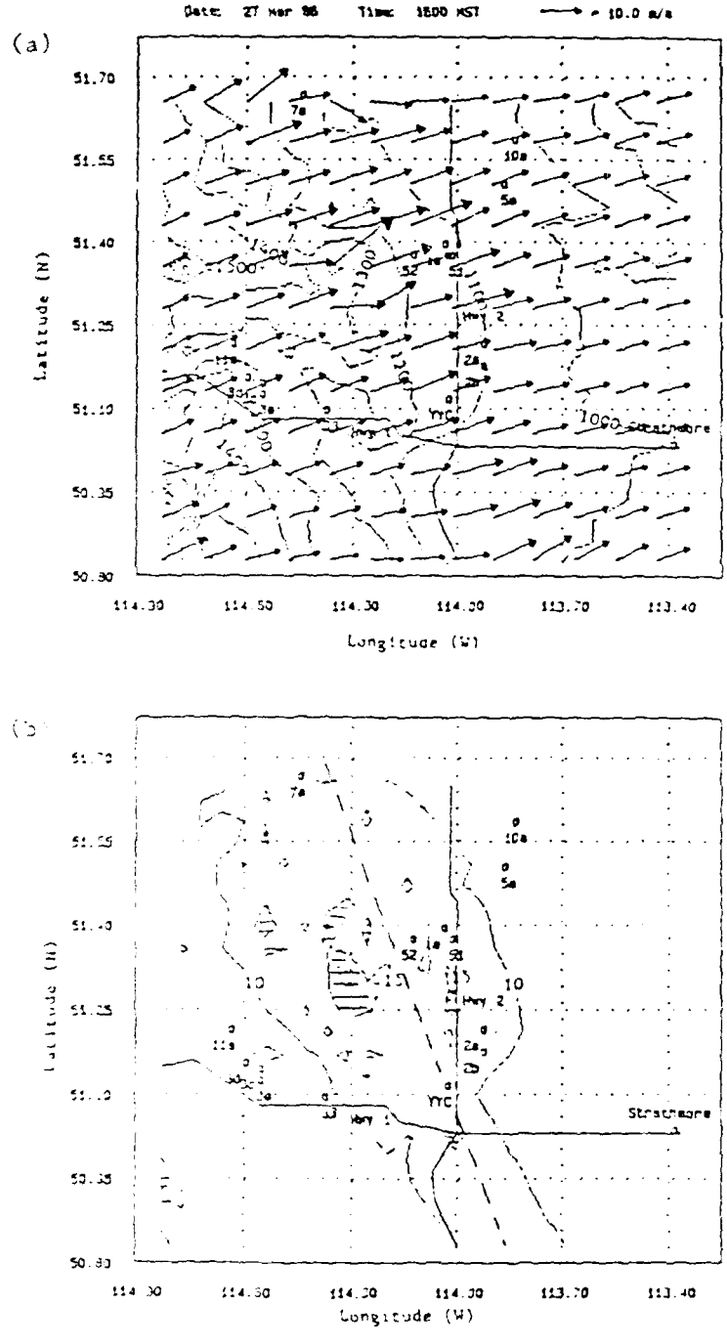

Figure 29. Same as Fig. 27, except for 1600 MST (Case Run #3).

to follow the 1200 m and 1300 m terrain contours.

As in the 3 November case, the highest model wind speeds are associated with the wave position through JPd (Fig. 27). Maximum model wind speed (30 m s^{-1}) occurs at 51.10N, 114.50W near JPd (stations 3c, 3d, and 3e).

As the wave trough is moved eastward to Btw (Fig. 28), areas of winds exceeding 20 m s^{-1} decrease in size and number. Maximum model wind speed occurs at 51.17N, 113.31W and decreases to 24 m s^{-1}.

As the wave trough reaches YYC (Fig. 29), the maximum model wind speed (25 m s^{-1}) is produced at 51.31N, 114.30W. The area of winds exceeding 15 m s^{-1} is larger than the previous case run, but areas of winds exceeding 20 m s^{-1} have further decreased in size and number.

A comparison of case runs #1, #2, and #3 (Figs. 27, 28, and 29) with the respective observed surface winds (Figs. 12, 13a, and 13b) shows that COMPLEX again accurately reproduces the high winds observed at the base of the major terrain slope for the case in which the wave trough is located through JPd. Although winds near Harmattan (station 7a) are also accurately reproduced, underestimates of observed wind speed occurs at virtually all other stations. In particular, model wind speeds are lower than observed winds at JPd for cases when the wave trough is located to the east, i.e., at Btw and YYC, at E. Crossfield (station

51), Crossfield #2 (station 2a), and Lone Pine Creek S. (station 5a) for all three case runs.

(3) Case Comparison and Discussion

A comparison of model output winds from the 3 November 1975 case (Figs. 24-26) with those from the 27 March 1986 case (Figs. 27-29) shows that greatest differences between the two cases appear downstream of the wave trough when it is located through JPd (Figs. 24 and 27) and Btw (Figs. 25 and 28). Downstream of the wave trough in the 27 March case, winds decrease sharply to a minima of < 10 m s^{-1}, while in the 3 November 1975 case, the decrease in wind speed is more gradual. Since identical flow surface configurations are used for both cases, differences between each case can be related to differences in the input surface and upper air wind data (Figs. 10-13, Table 2). For the 27 March 1986 case, the wind speed applied at the boundary layer top is 6 m s^{-1} less than that of the 3 November 1975 case. Additionally, surface wind data are not available from Carstairs (station 14) and surface wind speed at Harmattan (station 7a) was 3-5 m s^{-1} below values from the 3 November 1975 case. Collectively, in the 27 March 1986 case, lighter winds at the boundary layer top, and the weighting of the initial wind analysis by lighter winds at Harmattan appear to be the cause of decreased model wind speeds downstream of the wave trough.

Similarities between the two cases appear in all analyses along the wave trough axis and when the wave trough is located through YYC. For both cases, wind speed maxima occur at nearly the same locations just upstream of the wave trough. Locating the wave trough through YYC produces only slightly different wind speed and direction patterns for both cases. Along Highway 2 at 51.30N, model wind speed is higher for the 27 March 1986 case while at 51.60N, 114.25W, model wind speed is higher for the 3 November 1975 case. This difference appears to be related to differences in the input surface wind data. In the 27 March 1986 case, model winds respond to inputs from Crossfield #2 (station 2a) and Crossfield #3 (station 2b) which are not available for the 3 November 1975 case. Similarly, in the 3 November 1975 case, model winds respond to inputs from Carstairs (station 14) which are not available for the 27 March 1986 case.

In general, both case analyses showed increased surface wind flow due to mesoscale forcing of the boundary layer by a 'hydrostatic wave' and from smaller scale topographic effects. The horizontal extent of the increased model surface wind flow was shown to vary with the effective wavelength of the hydrostatic wave. Maximum model surface wind speeds occurred at the base of the principal terrain slope and were within 6-12% of the maximum observed surface wind speed.

Both analyses also displayed two general problems: (i) there were unrealistic changes in wind direction due to the lateral boundaries and (ii) there was considerable underestimation of observed wind speeds upwind of the wave trough as the wave progressed from JPd to YYC. To illustrate the wind speed underestimation problem, two west-east distributions of model wind speed through JPd, Spr, and YYC are presented in Fig. 30. These diagrams are constructed from the 27 March 1986 case when the hydrostatic wave trough axis was located through Btw (Fig. 30a) and YYC (Fig. 30b). Both modified (Fig. 30) and unmodified (Chapter 3) flow surface shapes were examined, however model wind speeds were still too low, i.e., the flow surface shape modification used in this study only slightly improves the model wind speed upwind of the wave trough position.

In reference to the latter problem, Durran and Klemp (1987) suggest that the amplification of downslope winds is fundamentally similar to the amplification produced during the transition from subcritical to supercritical flow in shallow-water hydraulic theory. Results from their non-hydrostatic, two-dimensional model indicate mesoscale forcing to be horizontally more extensive than that produced by a hydrostatic wave, as used in the present case. It is suggested that some sort of similar, 'hydraulic jump' forcing would eliminate the problems with underestimated wind speeds upstream of the mesoscale wave trough as dis-

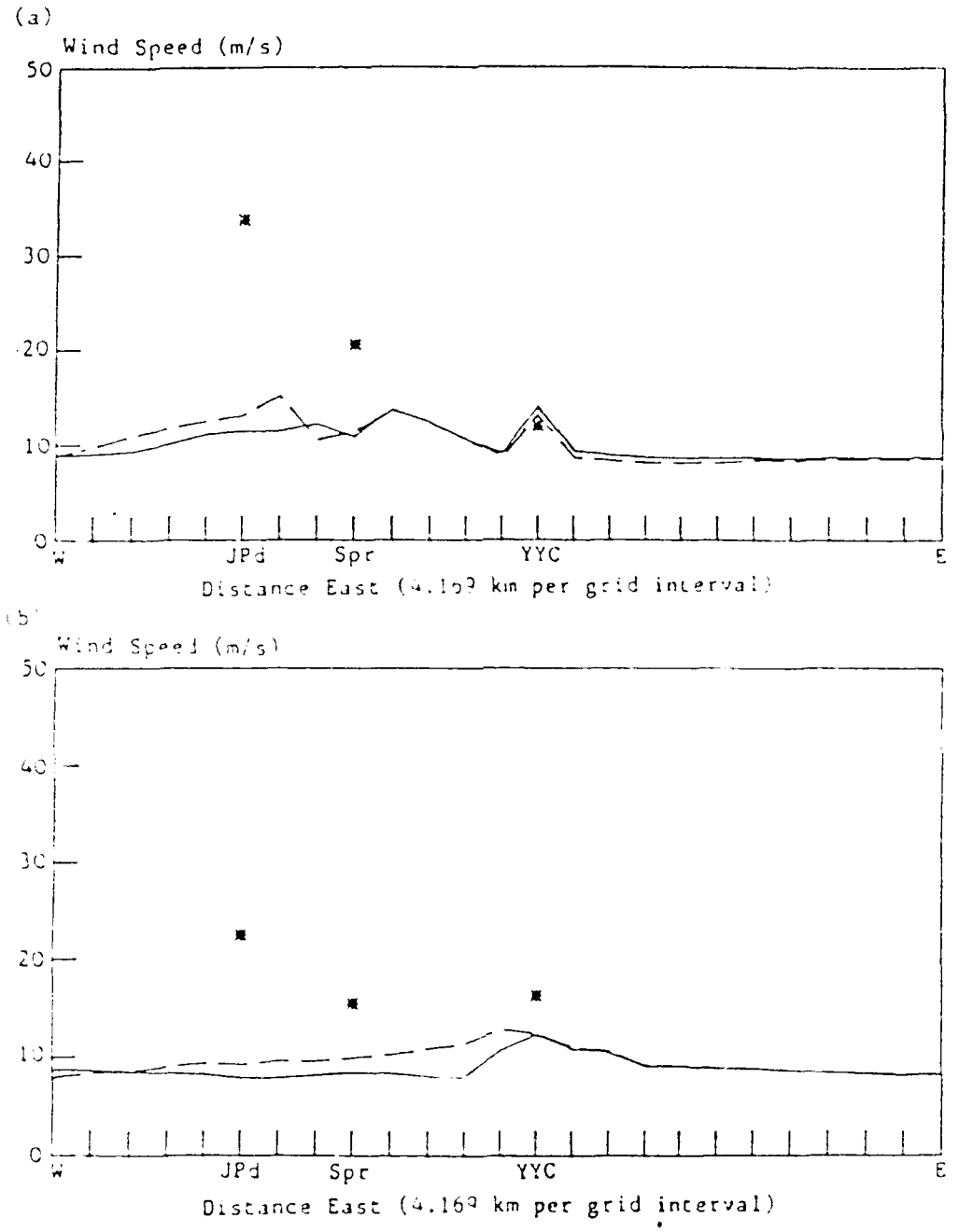

Figure 30. East-west variation of model anemometer height wind speed through Jumping Pound (JPd), Springbank (Spr), and Calgary International Airport (YYC) for modified (dashed line) and unmodified (solid line) flow surface configurations upstream of wave troughs located at (a) Btw and (b) YYC. Observed wind speeds are denoted by an asterisk (See text for discussion).

cussed above. Future experiments with COMPLEX may benefit from a modification of the boundary layer top to reflect the hydraulic jump configuration.

Chapter 5

SUMMARY, CONCLUSIONS, AND RECOMMENDATIONS FOR FUTURE RESEARCH

A mass-consistent, diagnostic wind model (COMPLEX) was modified to analyze flow during two Alberta chinook windstorm cases. The principal change to COMPLEX involved the modification of its flow-following coordinate system in order to simulate forcing of the surface wind flow by mountain waves. Specifically, the forcing was provided by a two-dimensional Gaussian exponential function derived from previously observed and simulated hydrostatic mountain wave patterns. The principal function variables were the average boundary layer thickness, and effective disturbance wavelength. Optimum values of the parameters were determined from a series of sensitivity tests.

The final analyses of the available surface wind data were accomplished by orienting the trough line of the two-dimensional hydrostatic wave parallel to the mountain crest at the point of the maximum observed surface winds. The analyses were then performed for each case at hourly intervals between the foothills and Calgary. Input data consisted of hourly averaged surface winds and 700 mb geostrophic winds.

In general, objective analysis with COMPLEX produced realistic wind distributions as the chinook windstorms progressed towards Calgary. Maximum winds during the wind-

storms were observed at the foot of the mountains and decreased as the windstorms moved eastward. Although as would be expected a COMPLEX surface isotach pattern arose due to terrain variations, the overall influence of the two-dimensional "hydrostatic" wave was clearly evident in the roughly symmetrical isotach pattern about the maximum winds near meso-scale wave trough.

A problem of unrealistic inflow and outflow at the lateral boundaries was also noted where the lower flow surface intersected the terrain. This problem can be easily minimized by keeping the model domain significantly larger than the area of interest.

The observed wind analyzed with COMPLEX were hourly average winds in the main, i.e., no consideration was given to gusts which may to exceed twice the hourly mean speed, especially in rugged terrain. In fact, the inability of COMPLEX to deal with turbulence and generally non hydrostatic phenomena which often characterize strong flow in mountainous terrain is probably the more questionable aspects of this application of the analysis technique.

Despite the limited success of this application of COMPLEX, it has been demonstrated to be a useful experimental tool. Furthermore, the economical utilization of COMPLEX on a small computer (IBM PC-AT) holds promise for wider research and operational applications.

These results indicate that the objective of this study has been reached, i.e., it has been shown that with appropriate modifications, a mass-consistent wind model for airflow in complex terrain (specifically, COMPLEX) can produce realistic analyses of strong surface winds during severe chinook windstorms. Furthermore, it appears that such analyses can be accomplished with a limited observational network and minimal computer resources. The analysis scheme presented here clearly holds promise for future operational applications. However, further experiments and modifications are necessary to eliminate some uncertainties in the technique.

The shape of the "hydrostatic lee wave" forcing function used in the current application did not reproduce the observed strong winds upstream of the lee wave trough axis. This suggests that the flow surfaces should have been lower in that area, resulting in an overall configuration comparable to previous numerical simulations of the atmospheric equivalent of a hydraulic jump, rather than a hydrostatic lee wave. Lacking detailed mesoscale observations of the flow surfaces, the use of a two-dimensional, time dependent, numerical model of the hydraulic jump to drive COMPLEX would go far in removing the arbitrary selection of the flow surface configuration (although microcomputer resources may be insufficient for such a modification).

COMPLEX should be further modified to reflect the well-mixed boundary layer which is characteristic of strong wind regimes. This change should not allow the intersection of the lowest flow surface and the terrain, thus eliminating the unrealistic pattern of strong winds around peaks rather than over them.

In some of the analyses described here, there was contamination of the wind field at the lateral boundaries of the domain. This problem can be minimized by simply increasing the size of the computational domain beyond the area of interest.

Finally, it is recommended that additional case studies with more observations should be considered to determine (i) the optimum distribution of observation stations, (ii) the errors introduced by non-hydrostatic effects, and (iii) the relationship between the modeled winds and the maximum gusts.

REFERENCES

Alaka, M. A., Ed., 1960: The airflow over mountains. WMO TN No. 34, Geneva, 115 pp.

Atkinson, B. W., 1981: Mesoscale Atmospheric Circulations. Academic Press, London, pp. 25-106.

Bedard, A. J. Jr., R. Nagle, and T. J. LeFebvre, 1981: Monostatic acoustic sounder measurements during Project Aeolus 1980: Case studies describing the erosion of surface-based stable layers. Proc. Int. Symp. on Remote Sensing of the Atmosphere and Oceans. 22-25 June 1981, Calgary, Alberta, VI: 27-57.

Bhumralkar, C. M., F. L. Ludwig, and R. L. Mancuso, 1978: Estimation of wind characteristics at potential wind energy conversion sites. Final report to Batelle-Northwest's Pacific Northwest Laboratory, Subcontract B-29105-A-E, SRI International Project 6537, Menlo Park, CA. 94025.

Blumen, W., and C. S. Hartsough, 1985: Reflection of hydrostatic gravity waves in a stratified shear flow. Part II: Application to downslope surface windstorms. J. Atmos. Sci., 42, 2319-2331.

Bretherton, F. P., 1969: Momentum transport by gravity waves. Quart J. Roy. Meteor. Soc., 95, 213-243.

Brinkmann, W. A. R., and I. Y. Ashwell, 1968: The structure and movement of the chinook in Alberta. Atmosphere, 6, 1-10.

Brinkmann, W. A. R., 1969: The definition of the chinook in the Calgary area. Unpublished M. Sc. Thesis, Department of Geography, University of Calgary.

Brinkmann, W. A. R., 1973: A climatological study of strong downslope winds in the Boulder area. NCAR Cooperative Thesis No. 27, INSTARR occasional paper No. 7, University of Colorado, 229 pp.

Brinkmann, W. A. R., 1974: Strong downslope winds at Boulder, Colorado. Mon. Wea. Rev., 102, 592-602.

Brown, J. M., 1986: A decision tree for forecasting downslope windstorms in Colorado. Preprint volume, Eleventh Conference on Weather Forecasting and Analysis, Kansas City, 7 pp.

Clark, T. L., and W. R. Peltier, 1977: On the evolution and stability of finite-amplitude mountain waves. J. Atmos. Sci., 34, 1715-1730.

Danielewicz, B., 1976: The structure and behavior of the chinook of southern Alberta. M.S. Thesis, Department of Geography, University of Calgary.

Drews, M. D., 1982: An aid to forecasting chinooks over southern Alberta. AES Technical memoranda TEL 880, Environment Canada, 9 pp.

Durran, D. R., 1986a: Another look at downslope windstorms. Part I. The development of analogs to supercritical flow in an infinitely deep, continuously stratified fluid. J. Atmos. Sci., 43, 2527-2543.

Durran, D. R., 1986b: Mountain waves. Mesoscale Meteorology and Forecasting, American Meteorological Society, Boston, 472-492.

Durran, D. R., and J. B. Klemp, 1987: Another look at downslope winds. Part II: Nonlinear amplification beneath wave-overturning layers. J. Atmos. Sci., 44, 3402-3412.

Endlich, R. M., 1967: An iterative method for altering the kinematic properties of wind fields. J. Appl. Meteor., 6, 837-844.

Endlich, R. M., F. L. Ludwig, C. M. Bhumralkar, and M. A. Estoque, 1980: A practical method for estimating wind characteristics at potential wind-energy conversion sites. Final report to Battelle-Northwest's Pacific Northwest Laboratory, Subcontract B-23149-A-E, SRI International Project 8349, Menlo Park, CA. 94025.

Endlich, R. M., F. L. Ludwig, C. M. Bhumralkar, and M. A. Estoque, 1982: A diagnostic model for estimating winds at potential sites for wind turbines. J. Appl. Meteor., 21, 1441-1454.

Endlich, R. M., and J. D. Lee, 1983: An improved diagnostic model for estimating wind energy. Prepared for Pacific Northwest Laboratory, Subcontract B-D5789-A-E, SRI International Project 4292, Menlo Park, CA. 94025.

Fingerhut, W. A., and P. F. Lester, 1973: Lower turbulent zones associated with mountain lee waves. Paper No. 30, Grant GA-32403, Dept. of Meteorology, San Jose State University, 118 pp.

Giusti, A., 1987: A climatological study of Alberta chinook windstorms, associated cross mountain pressure gradients, and upwind soundings. Paper presented at Fourth Conference on Mountain Meteorology, Seattle, WA., AMS, 4 pp.

Hoinka, K. P., 1985: Observation of the airflow over the Alps during a foehn event. Quart. J. R. Met. Soc., 111, 199-224.

Holmes, R. M., and K. D. Hage, 1971: Airborne observations of three chinook type situations in southern Alberta. J. Appl Meteor., 10, 1138-1153.

Houghton, D. D., and A. Kasahara, 1968: Nonlinear shallow fluid flow over an isolated ridge. Commun. Pure Appl. Math, 21, 1-23.

Hunt, J. R., and W. H. Snyder, 1980: Experiments on stably and neutrally stratified flow over a three-dimensional hill. J. Fluid Mech., 96, 671-704.

Huschke, R. E., Ed., 1959: Glossary of Meteorology. American Meteorological Society, Boston, pp. 373.

Ives, R. L., 1950: Frequency and physical effects of chinook winds in the Colorado high plains region. Annals Assoc. Amer. Geographers, 40, 293-327.

Julian, L. T., and P. R. Julian, 1969: Boulder's winds. Weatherwise, 22, 108-112 and 126.

Kellie, A. R., 1972: Low level atmospheric structure in Calgary in pre-chinook conditions. Unpublished M. Sc. Thesis, Department of Geography, University of Alberta.

Klemp, J. B., and D. K. Lilly, 1975: The dynamics of wave-induced downslope winds. J. Atmos. Sci., 32, 320-339.

Klemp, J. B., and D. K. Lilly, 1978: Numerical simulation of hydrostatic mountain waves. J. Atmos. Sci., 35, 78-107.

Kuettner, J. P., and T. H. R. O'Neill, 1981: ALPEX-the GARP mountain subprogram. Bull Am. Meteorol. Soc., 62, 793-805.

Leelananda, S. A., S. K. Aggarwal, and T. Mathews, 1981. Temperature and velocity turbulence during the onset of chinooks. Proc. Int. Symp. on Remote Sensing of the Atmosphere and Oceans. 22-25 June 1981, Calgary, Alberta, VI: 12-26.

Lester, P. F., 1975: A case study of the Alberta chinook. Presented at the 9th Annual Meeting of the Canadian Meteorological Society, Vancouver, British Columbia, 14 pp.

Lester, P. F., 1976a: The chinook of southern Alberta - a problem assessment. Presented to the 10th Congress of the Canadian Meteorological Society, Quebec City, Quebec, 14 pp.

Lester, P. F., 1976b: A quantitative definition of the chinook of southern Alberta. Environmental Sciences Centre, University of Calgary, 28 pp.

Lester, P. F., 1976c: Evidence of long lee waves in southern Alberta. Atmosphere, 14, 28-36.

Lester, P. F., 1976d: An observational and synoptic study of the chinook arch cloud. Environmental Sciences Centre, University of Calgary, 27 pp.

Lester, P. F., 1978a: A severe chinook windstorm. In Preprints, Conference on Sierra Nevada Meteorology, South Lake Tahoe, CA., American Meteorological Society.

Lester, P. F., 1978b: A lee wave cloud climatology for Pincher Creek, Alberta. Atmosphere-Ocean, 16, 157-168.

Lester, P. F., 1985: The Alberta chinook study: A plan for comprehensive study. Department of Meteorology, San Jose State University, 28 pp.

Lester, P. F., 1987: Personal communication.

Lester, P. F., and R. E. Bach Jr., 1986: An extreme clear air turbulence incident associated with a strong downslope windstorm. Presented at the 24th AIAA Aerospace Sciences Meeting, Reno, Nevada, 7 pp.

Lester, P. F., and J. I. MacPherson, 1977: Waves and turbulence in the vicinity of a chinook arch cloud. Mon. Wea. Rev., 105, 1447-1457.

Lester, P. F., and L. D. Phillips, 1987: Some synoptic and mesoscale characteristics of severe chinook windstorms in southern Alberta. Paper presented at Fourth Conference on Mountain Meteorology. Seattle, WA., AMS. 4 pp.

Lilly, D. K., 1972: Wave momentum flux-a GARP problem. Bull Amer. Met. Soc., 53, 17-23.

Lilly, D. K., 1978: A severe downslope windstorm and an aircraft turbulence event induced by a mountain wave. J. Atmos. Sci., 35, 59-77.

Lilly, D. K., and J. B. Klemp, 1980: Comments on "The evolution and stability of finite-amplitude mountain waves. Part II: Surface wave drag and severe downslope windstorms." J. Atmos. Sci., 37, 2119-2121.

Lilly, D. K., J. M. Nicholls, R. M. Chervin, P. J. Kennedy, and J. B. Klemp, 1982: Aircraft measurements of momentum flux over the Colorado Rocky Mountains. Quart. J. R. Met. Soc., 108, 625-642.

Lilly, D. K., and E. J. Zipser, 1972: The front range windstorm of 11 January 1972. Weatherwise, 25, 56-63.

Long, R. R., 1954: Some aspects of the flow of stratified fluids. Part II. Experiments with a two fluid system. Tellus, 6, 97-115.

Longley, R. W., 1967: The frequency of winter chinooks in Alberta. Atmosphere, 5, 4-16.

Ludwig, F. L., 1987: Personal communication.

Ludwig, F. L., R. M. Endlich, and K. C. Nitz, 1985: Inclusion of energy considerations in a mass-consistent wind interpolation scheme. Presented at the 6th Annual EOSAEL/TWI Conference, Las Cruces, New Mexico, 26 pp.

Lyra, G., 1943: Theorie der stationaren Leewellenströmung in freier atmosphare. Zeit. angew. Math. u. Mech. 23, 1-28.

Mass, C. F., and D. P. Dempsey, 1985: A one-level mesoscale model for diagnosing surface winds in mountainous and coastal regions. Mon. Wea. Rev., 113, 1211-1227.

Mathews, T., and R. Hicks, 1979: Typical features of atmospheric turbulence profiles associated with chinooks. Atmosphere-Ocean, 17, 125-134.

Mathews, T., P. F. Lester, and R. B. Hicks, 1984: SODAR observations of chinooks and arctic front passages along the eastern slope of the Canadian Rockies. Atmosphere-Ocean, 22, 328-342.

Miller, D. J., W. A. R. Brinkmann, and R. G. Barry, 1974: Wind Storms: A case study of wind hazard for Boulder, Colorado, in: G. F. White, Ed.: Natural Hazards: Local, National, and Global. Oxford University Press, New York.

Nicholls, J. M., 1973: The airflow over mountains. Research 1958-1972. WMO TN No. 127, 73 pp.

Nitz, K. C., R. M. Endlich, and F. L. Ludwig, 1985: User's guide for on-line software for wind-field analysis and display. Prepared for Pacific Gas and Electric Company, SRI International Project 7633, Menlo Park, CA. 94025.

Peltier, W. R., and T. L. Clark, 1979: The evolution and stability of finite-amplitude mountain waves. Part II. Surface wave drag and severe downslope winds. J. Atmos. Sci., 36, 1498-1529.

Peltier, W. R., and T. L. Clark, 1980: Reply. J. Atmos.Sci., 37, 2122-2125.

Queney, P., 1948: The problem of air flow over mountains: A summary of theoretical studies. Bull. Amer. Meteor. Soc., 29, 16-26.

Sangster, W. E., 1977: An updated objective forecast technique for Colorado downslope winds. NOAA TM NWS CR-6 Central Region Headquarters NWS, 23 pp.

Sasaki, Y., 1958: An objective analysis based on the variational method. J. Meteor. Soc. Japan, 36, 77-88.

Sasaki, Y., 1970: Some basic formalisms in numerical variational analysis. Mon. Wea. Rev., 98, 875-883.

Scheetz, V. R., J. F. Henz, and R. A. Maddox, 1976: Colorado severe downslope windstorms. Final Report under Contract No. 5-35421 to TDL/SDO/NWS from Geophysical Research and Development Corporation.

Scorer, R. S., 1949: Theory of waves in the lee of mountains. Quart. J. R. Met. Soc., 75, 41-56.

Scorer, R. S., and H. Klieforth, 1959: Theory of mountain waves of large amplitude. Quart. J. R. Met. Soc., 85, 131-143.

Sherman, C. A., 1978: A mass-consistent model for wind fields over complex terrain. J. Appl. Meteor., 17, 312-319.

Smith, R. B., 1980: ALPEX update. Bull. Am. Meteorol. Soc., 61, 136-138.

Smith, R. B., 1985: On severe downslope winds. J. Atmos. Sci., 42, 2597-2603.

Tredo, D. C. Jr., 1987: Application of a diagnostic boundary layer wind model to the San Francisco bay area. M.S. Thesis. Department of Meteorology, San Jose State University, 120 pp.